

Numerical evaluation of stress intensity factors and T-stress for interfacial cracks and cracks terminating at the interface without asymptotic enrichment

Sundararajan Natarajan^{a,1}, Chongmin Song^a, Salim Belouettar^b

^a*School of Civil and Environmental Engineering, The University of New South Wales, Sydney, NSW 2052, Australia.*

^b*Centre de Recherche Public Henri Tudor, 29, Avenue John F Kennedy, L-1855 Luxembourg-Kirchberg, Luxembourg.*

Abstract

In this paper, we extend the recently proposed extended scaled boundary finite element method (xSBFEM) [1] to study fracture parameters of interfacial cracks and cracks terminating at the interface. The approach is also applied to crack growth along the interface and crack deflecting into the material within the context of linear elastic fracture mechanics. Apart from the stress intensity factors, the T-stress can be computed directly from the definitions, without any requirement of path independent integrals. The method aims at improving the capability of the extended finite element method in treating crack tip singularities of cracks at interfaces. An optimum size of the scaled boundary region is presented for multimaterial junctions. The proposed method: (1) does not require special numerical integration technique; (2) does not require a priori knowledge of the asymptotic fields and (3) the stiffness of the region containing the crack tip is computed directly. The robustness of the proposed approach is demonstrated with a few examples in the context of linear elastic fracture mechanics. A discussion on the crack growth along the interface and crack deflecting into the material is also presented.

Keywords: scaled boundary finite element method, extended finite element method, interfacial crack, T-stress, stress intensity factor, enrichment functions, numerical integration.

1. Introduction

The finite element method (FEM) reformulates the continuous boundary and initial value problems into equivalent variational forms. The FEM requires the domain to be subdivided into non-overlapping regions called ‘elements’ and local polynomial representation is used for the fields within the element. The FEM with piecewise polynomials are inefficient to deal with internal discontinuities such as material interfaces or singularities. The material interfaces can be captured by a conforming mesh and the singularities can be captured by using quarter-point elements [2] or by locally enriching the finite element approximation space with singular functions [3]. In case of the quarter point elements, the singularity is captured by moving the element’s mid-side node to the position one quarter of the way from the crack tip. This was considered to be a major milestone in applying the FEM for linear elastic fracture mechanics (LEFM). Tracey [4] and Atluri *et al.*, [5]

¹School of Civil and Environmental Engineering, The University of New South Wales, Sydney, NSW 2052, Australia. Tel: +61(2)9385 5030. Email: s.natarajan@unsw.edu.au; sundararajan.natarajan@gmail.com

proposed a new element that has an inverse square root singularity near the crack. The main advantage of this element is that the stress intensity factors (SIFs) can be computed more accurately. Strang and Fix in their well known book [3], proposed to add singular functions to approximate the displacement field near the singularity. Benzley [6] developed an arbitrary quadrilateral element with singular corner node by ‘enriching’ a bilinear quadrilateral element with singular terms. All the above mentioned approaches still relies on a conforming finite element mesh. In an effort to overcome the limitations of the FEM, meshfree methods were introduced. Treatment of evolving discontinuities in meshfree methods is more straightforward because it does not require conforming mesh or mesh adaptation as the discontinuities evolve [7, 8, 9, 10, 11, 12]. Three dimensional crack propagation have been presented in [13, 14, 15, 16, 9, 17]. On another albeit related front, in the past decade reducing the meshing burden has spurred interest in the research community, whilst still retaining the finite element framework [18, 19, 20, 21, 22, 23]. Of particular note, in this study, we focus our attention on enrichment methods, especially, on the methods which are built on the finite element framework, for example, the extended FEM (XFEM). However, the idea presented here can be coupled with other methods, such as the meshless methods [24] and the boundary element method [25] to name a few.

Based on the seminal work of Babuška *et al.*, [18], Belytschko’s group in 1999 [19] introduced the XFEM that can model crack propagation and strong discontinuities with minimal remeshing. Since its inception, the XFEM has emerged as a versatile tool to handle internal discontinuous surfaces or moving boundaries independent of the underlying finite element discretization. Built on a finite element framework, the method relies on a modification (augmentation, enrichment) of the finite element spaces to capture the internal discontinuities. The success of the XFEM when applied to moving boundary problems, esp, crack growth, relies on the a priori knowledge of the set of functions that span the asymptotic fields ahead of the crack tip. The requirement for a priori knowledge of the asymptotic fields hinders the application of the XFEM directly to heterogeneous materials for which the asymptotic fields do not exist in closed form or are very complex. When the required functions are not known a priori, these functions can be computed numerically [26, 27, 28, 29, 30]. Nevertheless, all the approaches adopted in the literature depend on the following two steps:

- If the enrichment functions are unknown a priori, the enrichment functions are computed numerically, for example, the work of Menk and Bordas [28], Mousavi *et al.*, [29] and Zhu [31].
- The numerically computed functions are then used as enrichment functions within the XFEM/GFEM framework.

In addition to the requirement of the knowledge of asymptotic fields, augmenting these functions to the FE approximation basis leads to other difficulties such as, blending problem, numerical integration of enrichment functions, ill-conditioning and additional unknowns. Recent research has been directed towards improving the method by alleviating some of the aforementioned difficulties (for example, hybrid crack element [32], spider XFEM [33], hybrid analytical XFEM [34], stable GFEM [35], etc.) whilst the other focus has been in developing new enrichment functions when XFEM is applied to heterogeneous materials (for example, enrichment functions for orthotropic materials [36, 37, 38], for functionally graded materials [39], for crack at bimaterial interfaces [40, 41] and cracks terminating at the interface [42], to name a few). However, in spite of these advancements, to accurately evaluate the fracture parameters (such as the stress intensity factors and the T-stress), special techniques, such as path-independent integrals, are necessary [43, 44, 45, 46, 47].

1.1. Approach

In this paper, we study the singular stress states that exist in solids when discontinuities are present in the geometry and/or the mechanical properties of the material using the scaled boundary formulation. The scaled boundary formulation is then combined with the XFEM to study the fracture parameters, for example, the stress intensity factors (SIFs) and the T-stress. The salient feature is that the combined method does not require a priori knowledge of the asymptotic expansions of the displacements. Moreover, the stiffness of the region containing the crack tip can be computed directly, unlike, the method described in [28, 29, 26, 31], which requires a two step procedure.

1.2. Outline

The paper commences with a brief introduction to the extended finite element method (XFEM) in Section 2 and the scaled boundary finite element method (SBFEM) in Section 3. The coupling of the XFEM and the SBFEM is discussed in Section 4. Section 5 discusses the computation of the stress intensity factors (SIFs) and the T-stress in an isotropic and in a heterogeneous medium. Section 6 presents the displacement and stress modes and the order of singularity for various configuration using the scaled boundary formulation. The effectiveness of the coupled scaled boundary and XFEM is demonstrated with a few problems from linear elastic fracture mechanics. Also, the formulation is used to model crack growth along the interface and into the material. The concluding remarks are given in the last section.

2. Overview of the extended finite element method

Consider $\Omega \subset \mathbb{R}^2$, the reference configuration of a cracked linearly isotropic elastic body (see Figure 1). The boundary of Ω , denoted by Γ , is partitioned into three parts Γ_u, Γ_n and Γ_c , where Dirichlet condition is prescribed on Γ_u and Neumann condition is prescribed on Γ_n and Γ_c . The governing equilibrium equations for a 2D elasticity problem with internal boundary Γ_c defined in the domain Ω and bounded by Γ is

$$\nabla_s^T \boldsymbol{\sigma} + \mathbf{b} = \mathbf{0} \quad \in \quad \Omega \quad (1)$$

where $\nabla_s(\cdot)$ is the symmetric part of the gradient operator, $\mathbf{0}$ is a null vector, $\boldsymbol{\sigma}$ is the stress tensor and \mathbf{b} is the body force. The boundary conditions for this problem are:

$$\begin{aligned} \boldsymbol{\sigma} \cdot \mathbf{n} &= \bar{\mathbf{t}} & \text{on} & \Gamma_t \\ \mathbf{u} &= \bar{\mathbf{u}} & \text{on} & \Gamma_u \\ \boldsymbol{\sigma} \cdot \mathbf{n} &= \bar{\mathbf{t}} & \text{on} & \Gamma_c \end{aligned} \quad (2)$$

where $\bar{\mathbf{u}} = (\bar{u}_x, \bar{u}_y)^T$ is the prescribed displacement vector on the essential boundary Γ_u ; $\bar{\mathbf{t}} = (\bar{t}_x, \bar{t}_y)^T$ is the prescribed traction vector on the natural boundary Γ_t and \mathbf{n} is the outward normal vector. In this study, it is assumed that the displacements remain small and the strain-displacement relation is given by $\boldsymbol{\varepsilon} = \nabla_s \mathbf{u}$. Let us assume a linear elastic behaviour, the constitutive relation is given by $\boldsymbol{\sigma} = \mathbf{D} : \boldsymbol{\varepsilon}$, where \mathbf{D} is a fourth order elasticity tensor. The weak formulation of the static problem is then given by:

$$\text{find } \mathbf{u}^h \in \mathcal{U}^h \text{ such that } \forall \mathbf{v}^h \in \mathcal{V}^h \quad a(\mathbf{u}^h, \mathbf{v}^h) = \ell(\mathbf{v}^h) \quad (3)$$

where $\mathcal{U}^h \subset \mathcal{U}$ and $\mathcal{V}^h \subset \mathcal{V}$.

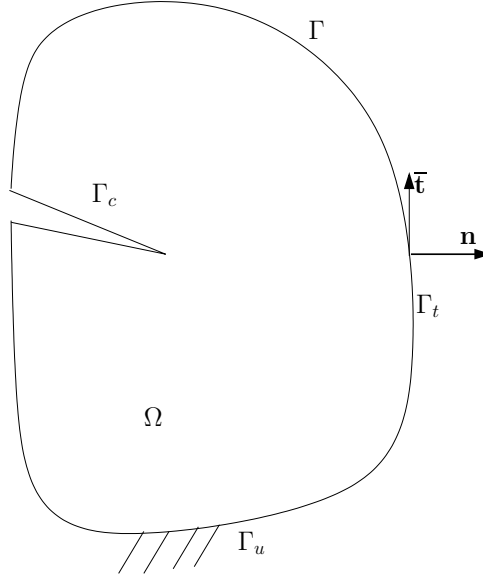


Figure 1: Two-dimensional elastic body with a crack.

2.1. *eXtended Finite Element Method (XFEM)*

In the XFEM, the classical FEM polynomial approximation space is augmented by a set of functions called the ‘enrichment functions’. This is achieved through the framework of the partition of unity. XFEM is classified as one of the partition of unity methods (PUMs). A partition of unity in a domain Ω is a set of functions N_I such that

$$\sum_{I \in \mathcal{N}^{\text{fem}}} N_I(\mathbf{x}) = 1, \quad \mathbf{x} \in \Omega \quad (4)$$

where \mathcal{N}^{fem} is the set of nodes in the FE mesh. Using this property, any function φ can be reproduced by a product of the PU shape functions with φ . Let $\mathbf{u}^h \in \mathcal{U}$, the XFEM approximation can be decomposed into the standard part $\mathbf{u}_{\text{fem}}^h$ and an enriched part $\mathbf{u}_{\text{enr}}^h$ as:

$$\mathbf{u}^h(\mathbf{x}) = \mathbf{u}_{\text{fem}}^h(\mathbf{x}) + \text{Enrichment functions} \quad (5)$$

where \mathcal{N}^{fem} is the set of all the nodes in the FE mesh. The modification of the displacement approximation does not introduce a new form of the discretized finite element equilibrium equations, but leads to an enlarged problem to solve. A generic form for the displacement approximation in case of the linear elastic fracture mechanics (LEFM) takes the form [19]:

$$\mathbf{u}^h(\mathbf{x}) = \sum_{I \in \mathcal{N}^{\text{fem}}} N_I(\mathbf{x}) \mathbf{q}_I + \sum_{J \in \mathcal{N}^c} N_J(\mathbf{x}) \vartheta(\mathbf{x}) \mathbf{a}_J + \sum_{K \in \mathcal{N}^f} N_K(\mathbf{x}) \sum_{\alpha=1}^n B_\alpha(r, \theta) \mathbf{b}_K^\alpha, \quad (6)$$

where \mathcal{N}^c is the set of nodes whose shape function support is cut by the crack interior (‘squared’ nodes in Figure 2) and \mathcal{N}^f is the set of nodes whose shape function support is cut by the crack tip (‘circled’ nodes in Figure 2). ϑ and B_α are the enrichment functions chosen to capture the displacement jump across the crack surface and the singularity at the crack tip and n is the total number of asymptotic functions. \mathbf{a}_J and \mathbf{b}_K^α are the nodal degrees of freedom corresponding to

functions ϑ and B_α , respectively. n is the total number of near-tip asymptotic functions and (r, θ) are the local crack tip coordinates. A priori knowledge of the shape functions is required for the successful application of the method. Since its inception, this has attracted researchers to investigate the enrichment functions that can accurately describe the asymptotic fields ahead of the crack tip [36, 38, 37, 42].

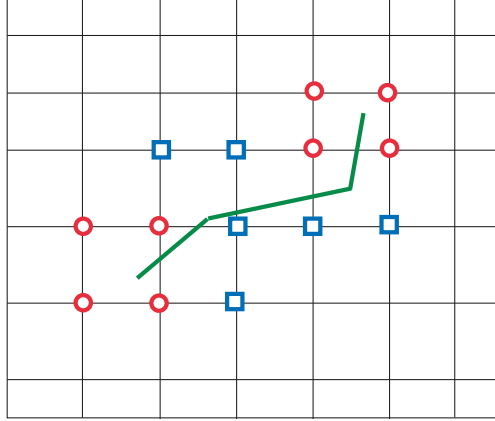


Figure 2: A typical FE mesh with an internal discontinuity. Nodes are enriched with a Heaviside functions whose nodal support is cut by the crack interior (*‘squared’* nodes) and with set of functions that span the asymptotic fields whose nodal support is cut by the crack tip (*‘circled’* nodes).

3. Overview of the scaled boundary formulation

The scaled boundary finite element method (SBFEM) is a semi-analytical computational technique developed by Wolf and Song [48]. It reduces the governing partial differential equations to a set of ordinary differential equations and is suitable for solving linear elliptic, parabolic and hyperbolic partial differential equations. In the SBFEM, the coordinates are defined by a radial-circumferential like coordinate system. Numerical solutions are sought around the circumferential direction using the conventional FEM, whilst in the radial direction, the solution is defined by smooth analytical functions. A scaling centre O is selected at a point from which the whole boundary of the domain is visible (see Figure 3). The radial coordinate ξ is defined from the scaling centre ($\xi = 0$) to the boundary ($\xi = 1$). Each edge on the boundary is discretised using 1D finite elements with local coordinate η , defined in the range $-1 \leq \eta \leq 1$. The coordinate of a point on the element $\mathbf{x}_\eta(\eta) = [x(\eta) \ y(\eta)]^T$ are expressed as

$$\mathbf{x}_\eta(\eta) = \mathbf{N}(\eta)\mathbf{x}_b \quad (7)$$

where \mathbf{x}_b are the coordinates of the nodes on the boundary and $\mathbf{N}(\eta)$ is the shape function matrix. In this study, standard 1D Gauss-Lobatto-Lagrange shape functions are used. By choosing the origin of the Cartesian coordinate system as the scaling center, the geometry of the domain is described as:

$$\mathbf{x}(\xi, \eta) = \xi \mathbf{x}_\eta(\eta) \quad (8)$$

Using Equation (8), the polar coordinates r and θ are expressed in the scaled boundary coordinates

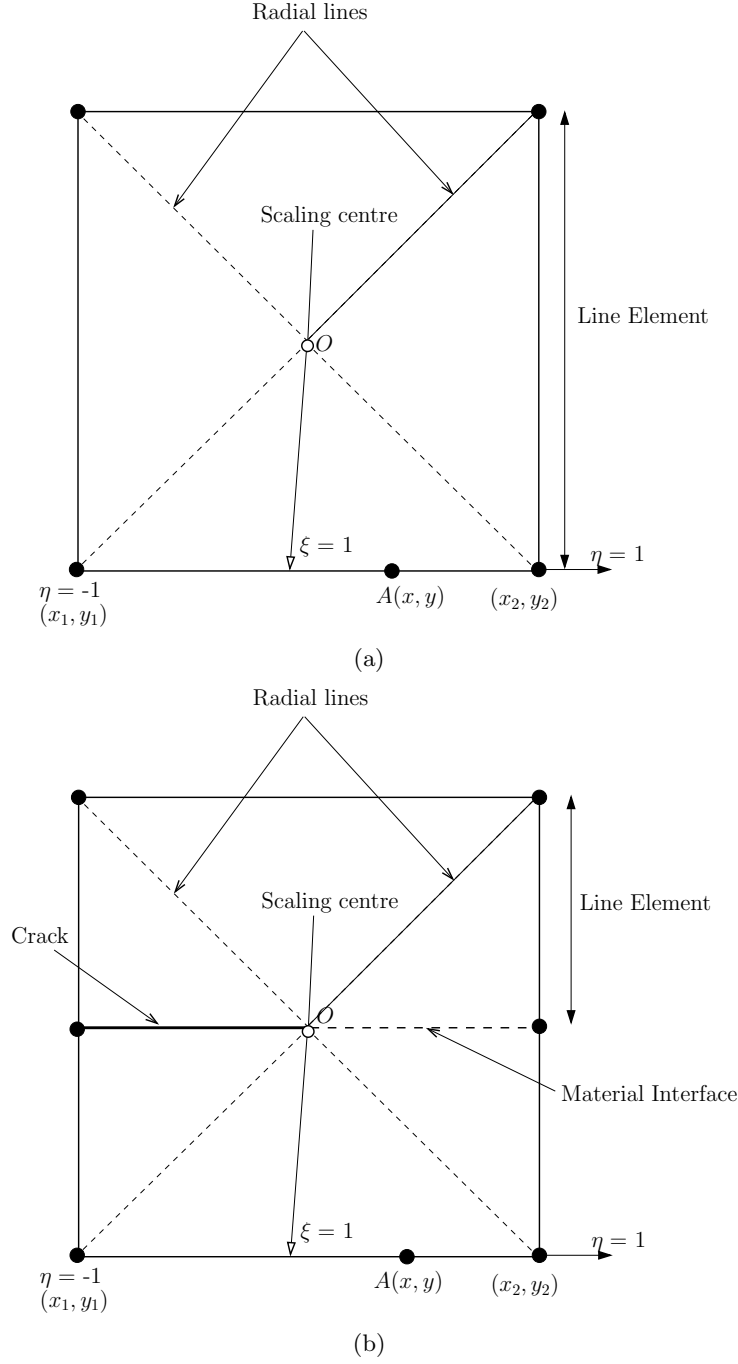


Figure 3: Coordinate transformation in the scaled boundary finite element method: (a) domain without a crack. The scaling centre O can be placed anywhere as long as it satisfies the visibility criteria and (b) domain with a crack and a material interface. The scaling center O is placed at the crack tip. The material interface within the domain need not be discretized, while on the boundary a conforming mesh is built with a node at the material interface.

ξ and η as

$$r(\xi, \eta) = \xi r_\eta(\eta) = \xi \sqrt{x_\eta^2(\eta) + y_\eta^2(\eta)} \quad (9)$$

$$\theta(\eta) = \arctan \frac{y_\eta(\eta)}{x_\eta(\eta)} \quad (10)$$

where $r_\eta(\eta)$ is the radial coordinate on the boundary. The angle $\theta(\eta)$ is a single-valued function in its principal value ($-\pi < \theta \leq \pi$). The element number and the local coordinate η can be regarded as a discrete representation of the angle θ .

Displacement approximation. The displacements of a point (for example, point A see Figure 3) is approximated by:

$$\mathbf{u}(\xi, \eta) = \mathbf{N}(\eta) \mathbf{u}(\xi) \quad (11)$$

where $\mathbf{u}(\xi)$ are the radial displacement functions. Substituting Equation (11) in the definition of strain-displacement relations, the strains $\boldsymbol{\varepsilon}(\xi, \eta)$ are expressed as:

$$\boldsymbol{\varepsilon}(\xi, \eta) = \mathbf{L} \mathbf{u}(\xi, \eta) \quad (12)$$

where \mathbf{L} is a linear operator matrix formulated in the scaled boundary coordinates as

$$\mathbf{L} = \mathbf{b}_1(\eta) \frac{\partial}{\partial \xi} + \xi^{-1} \mathbf{b}_2(\eta) \quad (13)$$

with

$$\begin{aligned} \mathbf{b}_1(\eta) &= \frac{1}{|\mathbf{J}(\eta)|} \begin{bmatrix} y_{\eta(\eta),\eta} & 0 \\ 0 & -x_{\eta(\eta),\eta} \\ -x_{\eta(\eta),\eta} & y_{\eta(\eta),\eta} \end{bmatrix} \\ \mathbf{b}_2(\eta) &= \frac{1}{|\mathbf{J}(\eta)|} \begin{bmatrix} -y_{\eta(\eta)} & 0 \\ 0 & x_{\eta(\eta)} \\ x_{\eta(\eta)} & y_{\eta(\eta)} \end{bmatrix} \end{aligned} \quad (14)$$

In Equation (14), $\mathbf{J}(\eta)$ is the Jacobian on the boundary [48, 49], given by:

$$\mathbf{J}(\eta) = \begin{bmatrix} x_{\eta(\eta)} & y_{\eta(\eta)} \\ x_{\eta(\eta),\eta} & y_{\eta(\eta),\eta} \end{bmatrix}$$

Using Equation (12) and the Hooke's law $\boldsymbol{\sigma} = \mathbf{D} \boldsymbol{\varepsilon}$, the stresses $\boldsymbol{\sigma}(\xi, \eta)$ is expressed as

$$\boldsymbol{\sigma}(\xi, \eta) = \mathbf{D} (\mathbf{B}_1(\eta) \mathbf{u}(\xi)_{,\xi} + \xi^{-1} \mathbf{B}_2(\eta) \mathbf{u}(\xi)) \quad (15)$$

where \mathbf{D} is the material constitutive matrix and

$$\begin{aligned} \mathbf{B}_1(\eta) &= \mathbf{b}_1(\eta) \mathbf{N}(\eta) \\ \mathbf{B}_2(\eta) &= \mathbf{b}_2(\eta) \mathbf{N}(\eta)_{,\eta} \end{aligned} \quad (16)$$

Substituting Equations (11), (12) and (15) for the displacement, strain and stress fields, respectively, in the virtual work statement results in [48, 49]

$$\begin{aligned} & \delta \mathbf{u}_b^T ((\mathbf{E}_0 \xi \mathbf{u}(\xi)_{,\xi} + \mathbf{E}_1^T \mathbf{u}(\xi))|_{\xi=1} - \mathbf{f}) \\ & - \int_0^1 \delta \mathbf{u}(\xi)^T (\mathbf{E}_0 \xi^2 \mathbf{u}(\xi)_{,\xi\xi} + (\mathbf{E}_0 + \mathbf{E}_1^T - \mathbf{E}_1) \xi \mathbf{u}(\xi)_{,\xi} - \mathbf{E}_2 \mathbf{u}(\xi)) d\xi = 0 \end{aligned} \quad (17)$$

where \mathbf{f} is the equivalent boundary nodal forces and \mathbf{u}_b is the nodal displacement vector. By considering the arbitrariness of $\delta \mathbf{u}(\xi)$, the following ODE is obtained:

$$\mathbf{E}_0 \xi^2 \mathbf{u}(\xi)_{,\xi\xi} + (\mathbf{E}_0 + \mathbf{E}_1^T - \mathbf{E}_1) \xi \mathbf{u}(\xi)_{,\xi} - \mathbf{E}_2 \mathbf{u}(\xi) = 0 \quad (18)$$

where \mathbf{E}_0 , \mathbf{E}_1 and \mathbf{E}_2 are coefficient matrices given by [48, 49]

$$\begin{aligned} \mathbf{E}_0 &= \int_{\eta} \mathbf{B}_1(\eta)^T \mathbf{D} \mathbf{B}_1(\eta) |\mathbf{J}(\eta)| d\eta, \\ \mathbf{E}_1 &= \int_{\eta} \mathbf{B}_2(\eta)^T \mathbf{D} \mathbf{B}_1(\eta) |\mathbf{J}(\eta)| d\eta, \\ \mathbf{E}_2 &= \int_{\eta} \mathbf{B}_2(\eta)^T \mathbf{D} \mathbf{B}_2(\eta) |\mathbf{J}(\eta)| d\eta. \end{aligned} \quad (19)$$

They are evaluated element-by-element on the element boundary and assembled similar to the standard FE procedure of assemblage. For a 2 noded line element, the coefficient matrices given by Equation (19) can be written explicitly. A simple routine is given in [1]. The code can easily be extended to treat higher order elements.

Computation of the stiffness matrix. Equation (18) is a homogeneous second-order ordinary differential equation. Its solution is obtained by introducing the variable $\chi(\xi)$

$$\chi(\xi) = \begin{Bmatrix} \mathbf{u}(\xi) \\ \mathbf{q}(\xi) \end{Bmatrix} \quad (20)$$

where $\mathbf{q}(\xi)$ is the internal load vector

$$\mathbf{q}(\xi) = \mathbf{E}_0 \xi \mathbf{u}(\xi)_{,\xi} + \mathbf{E}_1^T \mathbf{u}(\xi) \quad (21)$$

The boundary nodal forces are related to the displacement functions by:

$$\mathbf{f} = \mathbf{q}(\xi = 1) = (\mathbf{E}_0 \xi \mathbf{u}(\xi)_{,\xi} + \mathbf{E}_1^T \mathbf{u}(\xi))|_{\xi=1} \quad (22)$$

This allows Equation (18) to be transformed into a first order ordinary differential equation with twice the number of unknowns in an element as:

$$\xi \chi(\xi)_{,\xi} = -\mathbf{Z} \chi(\xi) \quad (23)$$

where \mathbf{Z} is a Hamiltonian matrix

$$\mathbf{Z} = \begin{bmatrix} \mathbf{E}_0^{-1} \mathbf{E}_1^T & -\mathbf{E}_0^{-1} \\ \mathbf{E}_1 \mathbf{E}_0^{-1} \mathbf{E}_1^T - \mathbf{E}_2 & -\mathbf{E}_1 \mathbf{E}_0^{-1} \end{bmatrix} \quad (24)$$

An eigenvalue decomposition of \mathbf{Z} is performed. The blocks of eigenvalues and transformation matrices necessary are:

$$\mathbf{Z} \begin{bmatrix} \Phi_u \\ \Phi_q \end{bmatrix} = \begin{bmatrix} \Phi_u \\ \Phi_q \end{bmatrix} \Lambda_n \quad (25)$$

In Equation (25), $\Lambda_n = \text{diag}(\lambda_1, \lambda_2, \dots, \lambda_n)$ contains the eigenvalues with negative real part. Φ_u and Φ_q are the corresponding transformation matrices of Λ_n . They represent the modal displacements and forces, respectively. The general solution of Equation (23) is given by:

$$\mathbf{u}(\xi) = \Phi_u \xi^{-\Lambda_n} \mathbf{c} \quad (26)$$

$$\mathbf{q}(\xi) = \Phi_q \xi^{-\Lambda_n} \mathbf{c} \quad (27)$$

where \mathbf{c} are integration constants that are obtained from the nodal displacements $\mathbf{u}_b = \mathbf{u}(\xi = 1)$ as:

$$\mathbf{c} = \Phi_u^{-1} \mathbf{u}_b \quad (28)$$

The complete displacement field of a point defined by the sector covered by a line element on the element is obtained by substituting Equation (27) into Equation (11) resulting in:

$$\mathbf{u}(\xi, \eta) = \mathbf{N}(\eta) \Phi_u \xi^{-\Lambda_n} \mathbf{c} \quad (29)$$

Taking the derivative of $\mathbf{u}(\xi)$ with respect to ξ and substituting into Equation (15) the stress field $\sigma(\xi, \eta)$ can be expressed as:

$$\sigma(\xi, \eta) = \Psi_\sigma(\eta) \xi^{-\Lambda_n - \mathbf{I}} \mathbf{c} \quad (30)$$

where the stress mode $\Psi_\sigma(\eta)$ is defined as:

$$\Psi_\sigma(\eta) = \mathbf{D} (-\mathbf{B}_1(\eta) \Phi_u \Lambda_n + \mathbf{B}_2(\eta) \Phi_u) \quad (31)$$

The stiffness matrix of an element is obtained by first substituting Equation (28) into Equation (27) at $\xi = 1$. This results in:

$$\mathbf{f} = \Phi_q \Phi_u^{-1} \mathbf{u}_b \quad (32)$$

From Equation (32), the stiffness matrix \mathbf{K} can be identified to be given by the expression

$$\mathbf{K} = \Phi_q \Phi_u^{-1} \quad (33)$$

Remark 1. *No a priori knowledge of the asymptotic solution and special integration technique is required to compute the stiffness matrix. The SBFEM solution includes the stress singularity as well. The details are given in Section 5.*

Remark 2. *The SBFEM can be formulated over arbitrary regions, for example over polygonal*

elements [50, 51].

4. Coupling of the XFEM & the SBFEM

Recently, the authors proposed the extended SBFEM (xSBFEM) [1]. The main idea of the xSBFEM is to approximate the non-smooth behaviour in the close vicinity by the scaled boundary formulation instead of augmenting the approximation basis with asymptotic expansion. The nodes whose nodal support is completely cut by the crack interior or the material interface are treated within the XFEM framework and enriched with a Heaviside function or 'abs' enrichment function. The scaling center is chosen as the crack tip (see Figure 4). This local modification and enrichment strategy introduces four types of elements:

- *Split elements* are elements completely cut by the crack interior or by the material interface. Their nodes are enriched with the Heaviside function to represent the jump across the crack face or by the 'abs' function to represent the weak discontinuity.
- *Split-blending elements* are elements neighbouring split elements. They are such that some of their nodes are enriched with the weakly discontinuous function and others are not enriched at all.
- *Scaled boundary elements* are elements in the close proximity of the crack tip treated by the semi-analytical formulation.
- *Standard elements* are elements that are in neither of the above categories. None of their nodes are enriched.

Remark 3. It is noted that no special treatment is required for the elements that share nodes between the Ω^{fem} and Ω^{sbfem} .

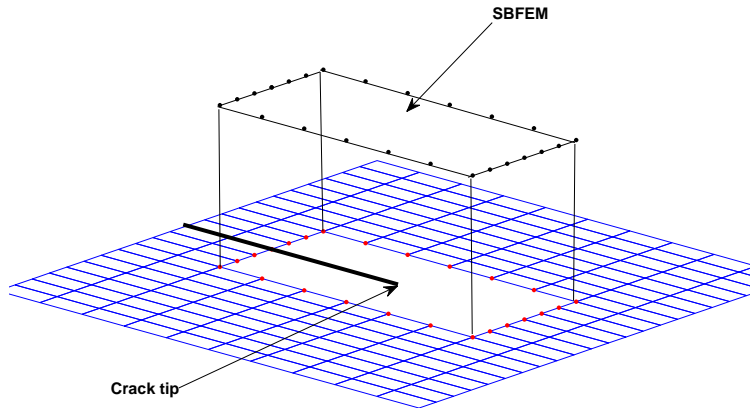


Figure 4: Coupling of XFEM and SBFEM

The displacement approximation can be decomposed into the standard part $\mathbf{u}_{\text{std}}^h$ and an enriched part $\mathbf{u}_{\text{xfem}}^h$ as given by Equation (6) without asymptotic enrichments. In the proposed approach, the standard part is further decomposed into the standard FEM $\mathbf{u}_{\text{fem}}^h$ and into a semi-analytical part $\mathbf{u}_{\text{sbfem}}^h$. The displacement approximation is then given by:

$$\mathbf{u}^h(\mathbf{x}) = \begin{cases} \sum_{I \in \mathcal{N}^{\text{fem}}} N_I(\mathbf{x}) \mathbf{q}_I + \sum_{J \in \mathcal{N}^c} N_J(\mathbf{x}) H(\mathbf{x}) \mathbf{a}_J & \mathbf{x} \in \Omega^{\text{fem}} \cup \Omega^{\text{xfem}} \\ \sum_{K \in \mathcal{N}^{\text{sbfem}}} N_K(\eta) \mathbf{u}_{bK}(\xi) & \mathbf{x} = f(\xi, \eta) \in \Omega^{\text{sbfem}} \end{cases} \quad (34)$$

where \mathcal{N}^{fem} is the set of all nodes in the FE mesh that belongs to Ω^{fem} , $\mathcal{N}^{\text{sbfem}}$ is the set of nodes in the FE mesh that belongs to Ω^{sbfem} and $\mathcal{N}^{\text{xfem}}$ is the set of nodes that are enriched with the Heaviside function H . N_I and N_J are the standard finite element functions, \mathbf{q}_I and \mathbf{a}_J are the standard and the enriched nodal variables associated with node I and node J , respectively. \mathbf{u}_{bK} are the nodal variables associated with the nodes on the boundary of Ω^{sbfem} and N_K are the standard FE shape functions defined on the scaled boundary coordinates in Ω^{sbfem} . For the nodes that on the boundary of Ω^{fem} and Ω^{sbfem} , no special coupling technique is required. As the nodal unknown coefficients are required to be continuous across the boundary, the unknown coefficients from the SBFEM and the FEM are the same and are assembled in the usual way. A similar procedure is followed when assembling the Ω^{fem} and Ω^{xfem} to the global stiffness and to the global force vector. For more details, interested readers are referred to [1].

5. Computation of the stress intensity factors and the T-Stress

An attractive feature of the SBFEM is that no a priori knowledge of the asymptotic solution is required to accurately handle the stress singularity at a crack tip. When the scaling centre is placed at the crack tip, the solution for the stress field in Equation (30) is expressed, by using Equation (9), as

$$\boldsymbol{\sigma}(r, \eta) = \sum_{i=1}^n c_i r^{-(\lambda_i+1)} \left(r_{\eta}^{\lambda_i+1}(\eta) \boldsymbol{\psi}_{\sigma i}(\eta) \right) \quad (35)$$

where $\boldsymbol{\psi}_{\sigma i}(\eta)$ is the i -th stress mode, i.e. the i -th column of the matrix $\boldsymbol{\Psi}_{\sigma}(\eta)$. Like the well-known William expansion [52], Equation (35) is a power series of the radial coordinate r . The radial variation of each term of the series is expressed analytically by the power function $r^{-(\lambda_i+1)}$. At discrete points along the boundary, the angular coordinates (see Equation (10)) are arranged as a vector $\boldsymbol{\theta}(\eta)$ and the stress modes $\boldsymbol{\psi}_{\sigma i}(\eta)$ are computed. $\boldsymbol{\psi}_{\sigma i}(\eta)$ and $\boldsymbol{\theta}(\eta)$ form a parametric equation of the angular variation of stresses. The singular stress and the T-stress terms can be easily identified by the value of the exponent $-(\lambda_i+1)$. When the real part of the exponent $-(\lambda_i+1)$ of a term is negative, the stresses of this term at the crack tip, i.e. $\xi = 0$, tend to infinity. When the exponent $-(\lambda_i+1)$ of a term is equal to 0, the stresses of this term are constant and contribute to the T-stress.

Crack in homogeneous material or material interface. In the case of a crack in a homogeneous material or on a material interface, two singular terms exist in the solution. Denoting the singular stress modes as I and II , the singular stresses $\boldsymbol{\sigma}^s(\xi, \eta)$ (superscript s for singular stresses) are

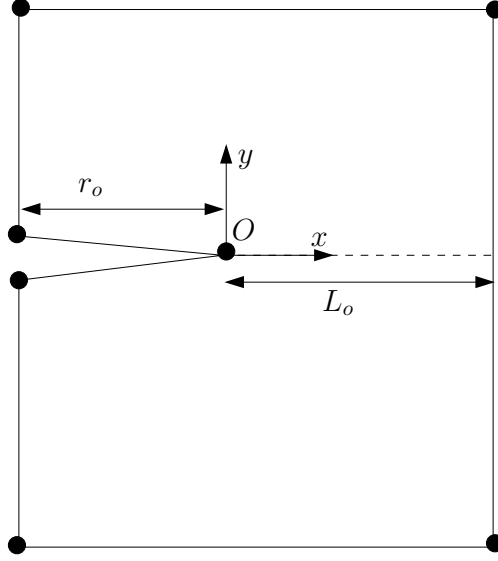


Figure 5: A cracked domain modelled by the scaled boundary finite element method. $L_o = r_\eta(\theta = 0)$ is the distance from the crack tip to the boundary. At the boundary $\xi = 1$.

obtained from Equation (35):

$$\boldsymbol{\sigma}^s(r, \eta) = \sum_{i=I,II} c_i r^{-(\lambda_i+1)} \left(r_\eta^{\lambda_i+1}(\eta) \boldsymbol{\psi}_{\sigma i}(\eta) \right) \quad (36)$$

Note that the singular stress terms are separated from other terms and the stress singularity is represented analytically. This allows the evaluation of the stress intensity factors by directly matching their definition with the singular stresses. For convenience, the point on the boundary along the crack front $\theta = 0$ (see Figure 5) is considered. The distance from the crack tip to the boundary is denoted as $L_o = r_\eta(\theta = 0)$. From Equation (36), the values of the singular stresses at this point are equal to:

$$\boldsymbol{\sigma}^s(L_o, \theta = 0) = \sum_{i=I,II} c_i \boldsymbol{\psi}_{\sigma i}(\theta = 0) \quad (37)$$

where $\boldsymbol{\psi}_{\sigma i}(\theta = 0)$ is the value of the stress modes at $\theta = 0$. It is obtained by interpolating $\boldsymbol{\psi}_{\sigma i}(\eta)$ at the discrete points of $\boldsymbol{\theta}(\eta)$.

Stress intensity factors can be computed directly from their definition using the stresses in Equation (37). For a crack in a homogeneous medium, the classical definition of stress intensity factors K_I and K_{II} for mode I and II are expressed as:

$$\begin{Bmatrix} K_I \\ K_{II} \end{Bmatrix} = \sqrt{2\pi r} \begin{Bmatrix} \sigma_{\theta\theta}^s(r, \theta = 0) \\ \tau_{r\theta}^s(r, \theta = 0) \end{Bmatrix} \quad (38)$$

Formulating Equation (38) at $r = L_o$ results in

$$\begin{Bmatrix} K_I \\ K_{II} \end{Bmatrix} = \sqrt{2\pi L_o} \begin{Bmatrix} \sigma_{\theta\theta}^s(L_o, \theta = 0) \\ \tau_{r\theta}^s(L_o, \theta = 0) \end{Bmatrix} \quad (39)$$

The stress intensity factors are then determined by substituting the stress components $\sigma_{\theta\theta}^s(L_o, \theta = 0)$ and $\tau_{r\theta}^s(L_o, \theta = 0)$ obtained from Equation (37) into Equation (39).

Crack at an interface. In the case of a crack at the interface between two isotropic materials, the orders of singularity are a pair of complex conjugates $0.5 \pm i\epsilon$, where the oscillatory index ϵ depends on the material properties. The stress intensity factors are defined as:

$$\begin{Bmatrix} K_I \\ K_{II} \end{Bmatrix} = \sqrt{2\pi r} \begin{bmatrix} \cos(\epsilon \ln(r/L)) & \sin(\epsilon \ln(r/L)) \\ -\sin(\epsilon \ln(r/L)) & \cos(\epsilon \ln(r/L)) \end{bmatrix} \begin{Bmatrix} \sigma_{\theta\theta}^{(s)}(r, 0) \\ \tau_{r\theta}^{(s)}(r, 0) \end{Bmatrix} \quad (40)$$

where L is the characteristic length. Formulating the definition (see Equation (40)) at $r = L_o$, the stress intensity factors are expressed as

$$\begin{Bmatrix} K_I \\ K_{II} \end{Bmatrix} = \sqrt{2\pi L_o} \begin{bmatrix} \cos(\epsilon \ln(L_o/L)) & \sin(\epsilon \ln(L_o/L)) \\ -\sin(\epsilon \ln(L_o/L)) & \cos(\epsilon \ln(L_o/L)) \end{bmatrix} \begin{Bmatrix} \sigma_{\theta\theta}^{(s)}(L_o, 0) \\ \tau_{r\theta}^{(s)}(L_o, 0) \end{Bmatrix} \quad (41)$$

where the singular stresses are obtained from Equation (37). Although, it is out of the scope of this paper, it is worthwhile to mention that the scaled boundary finite element method is capable of modeling all types of stress singularity occurring at multi-material junctions [53].

For a subdomain containing a crack tip, two of the eigenvalues are equal to 1. They represent the T -stress term and the rotational rigid body motion term, which does not contribute to the stresses. They are separated from other terms in Equation (37) and expressed as (superscript T for the T -stress)

$$\boldsymbol{\sigma}^T(\eta) = \sum_{i=T_I, T_{II}} c_i \boldsymbol{\psi}_{\sigma_i}(\eta) \quad (42)$$

The T-stress along the crack front ($\theta = 0$) is determined by interpolating the angular variation of the two stress modes ($\boldsymbol{\theta}(\eta), \boldsymbol{\psi}_{\sigma_i}(\eta)$).

Remark 4. *Note that when evaluating the stress intensity factors or the T -stress, only the corresponding modes are involved. It is not necessary to evaluate the complete stress field.*

6. Results and discussion

In this section, we first employ the SBFEM to estimate the order of the singularity and the stress and the displacement modes for known benchmark problems in the context of linear elastic fracture mechanics. Later, we will adopt the combined XFEM and the SBFEM to compute the stress intensity factors and the T-stress for cracks aligned to the material interfaces. The stress distribution ahead of the crack and the T-stress for a crack terminating at an interface is also studied. The results of which are compared with a finite element solution. In this study, unless otherwise mentioned, bilinear quadrilateral elements are used. An extension to other arbitrary polytopes is possible as illustrated in [51]. The results from the present approach are compared with available numerical results in the literature, for example, with the XFEM [54] and with the BEM [55, 56].

6.1. Computation of displacement & stress modes and the order of singularity

To test and to demonstrate the convergence and the accuracy of the SBFEM in estimating the strength of the singularity and the corresponding displacement and stress modes, we consider three examples.

Crack in an isotropic medium. Figure 6 shows a crack in an isotropic medium with Young's modulus E and Poisson's ratio ν . The displacement fields are given by [52]:

$$\begin{aligned} u_x(r, \theta) &= \frac{K_I}{2\mu} \sqrt{\frac{r}{2\pi}} \cos \frac{\theta}{2} \left[\kappa - 1 + 2 \sin^2 \frac{\theta}{2} \right] + \frac{K_{II}}{2\mu} \sqrt{\frac{r}{2\pi}} \sin \frac{\theta}{2} \left[\kappa + 1 + 2 \cos^2 \frac{\theta}{2} \right] \\ u_y(r, \theta) &= \frac{K_I}{2\mu} \sqrt{\frac{r}{2\pi}} \sin \frac{\theta}{2} \left[\kappa + 1 - 2 \cos^2 \frac{\theta}{2} \right] + \frac{K_{II}}{2\mu} \sqrt{\frac{r}{2\pi}} \cos \frac{\theta}{2} \left[\kappa - 1 - 2 \sin^2 \frac{\theta}{2} \right] \end{aligned} \quad (43)$$

where κ is the Kolosov constant and μ is the shear modulus. The reference solution is obtained along a circle of unit radius $r = 1$ and with stress intensity factors K_I is set to unity and K_{II} to zero. The displacement modes, the stress modes and the order of singularity are computed by the scaled boundary formulation. A typical scaled boundary finite element mesh is shown in Figure 6. It is noted that only the boundary of the domain needs to be discretized and the solution within the domain is represented analytically.

Remark 5. *In our study, we have employed spectral element to discretize the boundary. We employ Lagrange interpolants within each element, where the nodes of these shape functions are placed at the zeros of Legendre polynomials (Gauss Lobatto points) mapped from the reference domain $[-1, 1] \times [-1, 1]$ to each element.*

In Table 1, the convergence of the order of singularity with increasing number of elements is shown. With decreasing element size, it is seen that the numerically estimated order of singularity converges to the theoretical value 0.5. Also, the influence of the order of the shape functions on the convergence of the order of singularity is shown. As expected, the theoretical value of 0.5 can be achieved by either increasing the order of the shape functions or by decreasing the element size. Figure 7 shows the relative error in the displacement norm for each component (i.e., u_x and u_y) with the increasing number of elements along the boundary. It can be seen that increasing the number of elements leads to decreasing error.

Equation (35) is the parametric equation for the stress field in the polar coordinates r and θ . The terms $(r_\eta^{\lambda_i+1}(\eta)\psi_{\sigma_i}(\eta))$ in Equation (35) together with $\theta(\eta)$ in Equation (10) are the stress modes describing the angular stress distribution at a constant radial coordinate r . Figure 8 shows the stress distribution ahead of the crack tip for mode I fracture problem. Each of the stress mode is normalized with its value of σ_{yy} at $\theta = 0^\circ$. A total of 8 third order elements were used to discretize the boundary. The results from the scaled boundary formulation are compared with the analytical solutions (represented by the superscript E). A very good agreement is observed.

Table 1: Convergence of the order of singularity for an isotropic plate with a crack.

| Number of Elements | Order of shape functions | | | |
|-----------------------|--------------------------|------------|------------|------------|
| | $p=2$ | $p=3$ | $p=4$ | $p=5$ |
| 8 | 0.50826515 | 0.50007949 | 0.49995729 | 0.50000291 |
| 40 | 0.50035216 | 0.49999979 | 0.50000000 | 0.50000000 |
| 80 | 0.50008862 | 0.49999999 | - | - |
| 160 | 0.50002219 | 0.50000000 | - | - |

Crack aligned to a bi-material interface. The second test case is a crack aligned to the bimaterial interface. Figure 9 shows the geometry and the corresponding finite element mesh. Again, only the

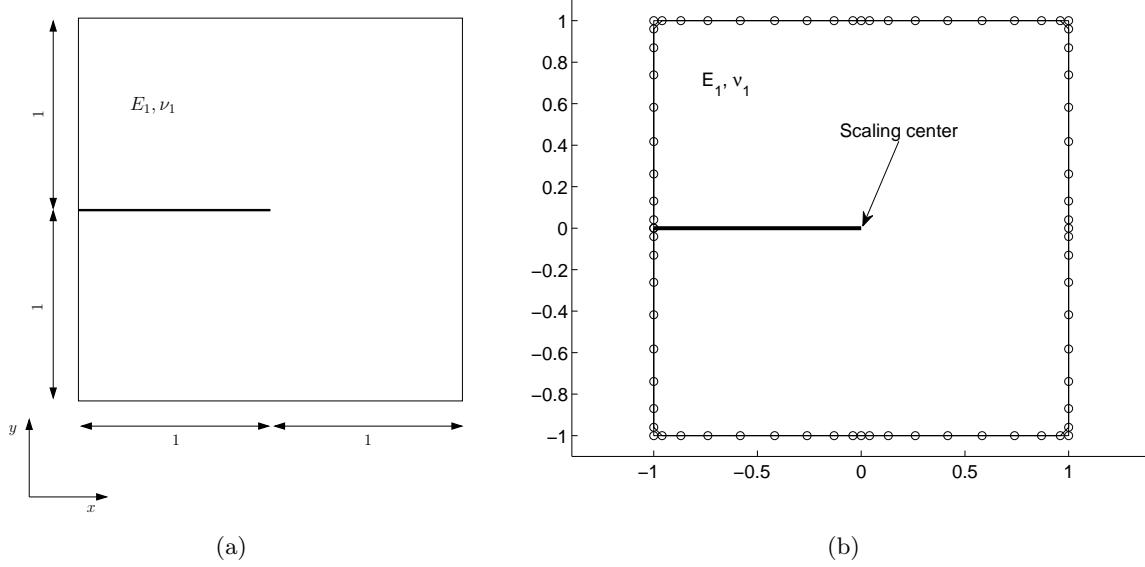


Figure 6: Crack in an isotropic medium: (a) geometry and (b) SBFEM Mesh detail

boundary of the domain is discretized. The Lagrange shape functions of order $p = 9$ and a total of eight elements are used to discretize the domain in the circumferential direction. The order of the singularity computed from the semi-analytical approach is compared with the analytical expression given by, $0.5 \pm i\epsilon$, where ϵ is the oscillatory index given by:

$$\epsilon = \frac{1}{2\pi} \log \left(\frac{1 - \beta}{1 + \beta} \right) \quad (44)$$

where β is the second Dundur's parameter

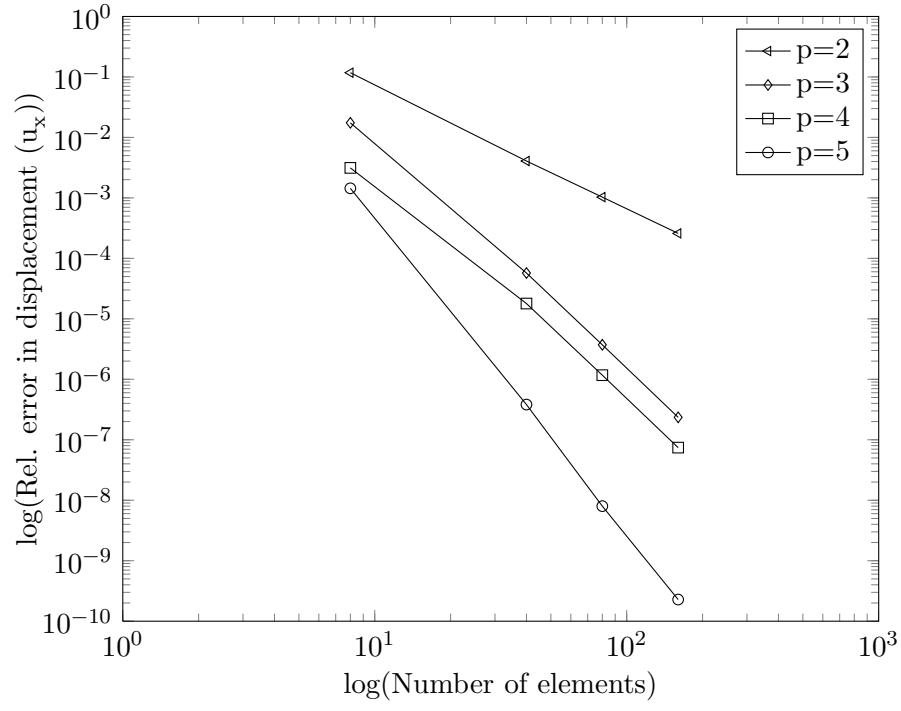
$$\beta = \frac{\mu_1(\kappa_2 - 1) + \mu_2(\kappa_1 - 1)}{\mu_1(\kappa_2 + 1) + \mu_2(\kappa_1 + 1)} \quad (45)$$

and,

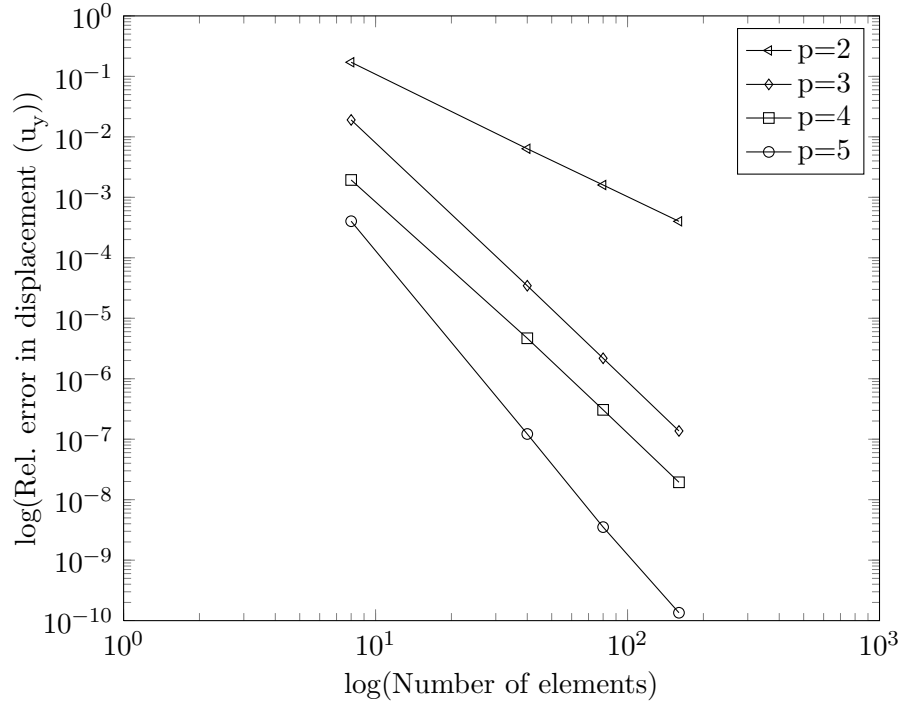
$$\kappa_i = \begin{cases} (3 - \nu_i)/(1 + \nu_i) & \text{plane stress} \\ 3 - 4\nu_i & \text{plane strain} \end{cases} \quad (46)$$

where μ_i, ν_i and $\kappa_i, (i = 1, 2)$ are the shear modulus, Poisson's ratio and the Kolosov coefficient, respectively. Figure 10 shows the influence of the ratio of Young's modulus on the order of the singularity. The angular stress distribution ahead of the crack aligned to a bimaterial interface is shown in Figure 11. The ratio of Young's modulus is $E_1/E_2 = 10$. The singular stress fields are obtained for a crack length $a = 0.5$ and $K_I/p\sqrt{\pi a} = 1.123$ and $K_{II}/p\sqrt{\pi a} = -0.123$. A very good agreement is observed.

Triple junction. As a last example, we consider the two specific cases of a triple junction: (a) a fully bonded triple junction and (b) a triple junction with a crack aligned to one of the interfaces. Figure 12 shows the problem description and the corresponding SBFEM mesh. Note that only the boundary of the domain needs to be discretized with 8 elements (on the boundary) with Lagrange



(a) Relative error in displacement, u_x



(b) Relative error in displacement, u_y

Figure 7: Crack in an isotropic medium: Convergence in the relative error in the displacement.

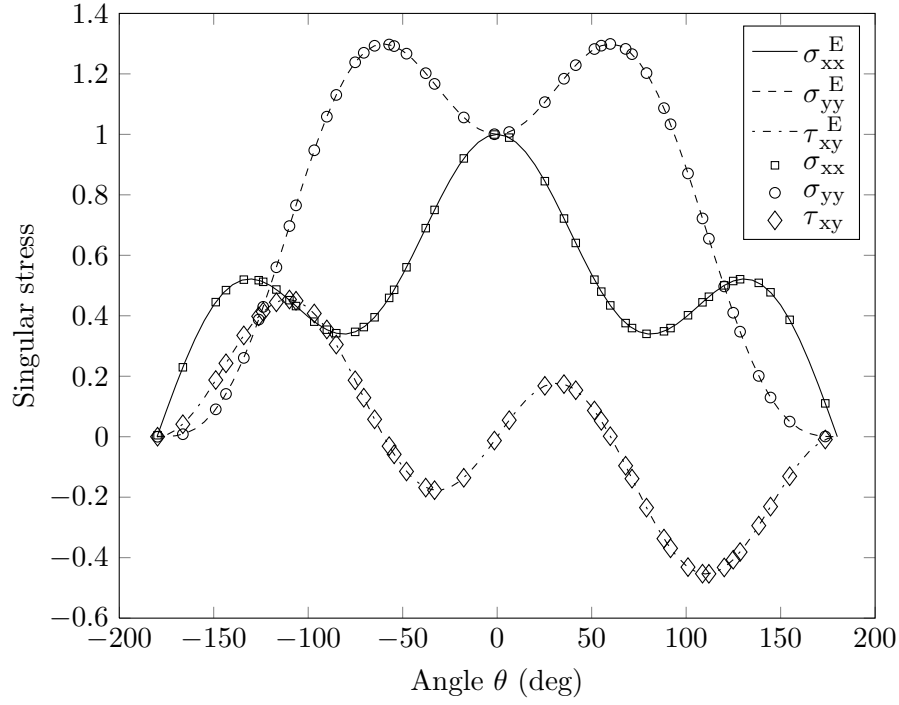


Figure 8: Angular distribution of singular stress ahead of a crack tip for a crack in an isotropic medium under mode I loading conditions, i.e., $K_I = 1$ and $K_{II} = 0$.

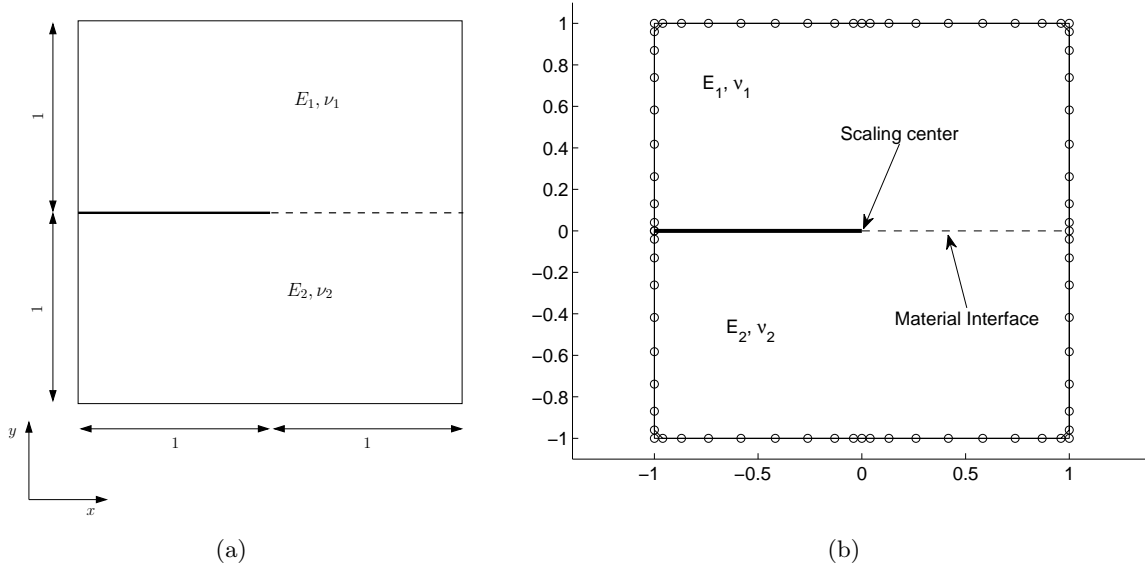


Figure 9: Crack aligned to a bi-material interface: (a) geometry and (b) SBFEM Mesh

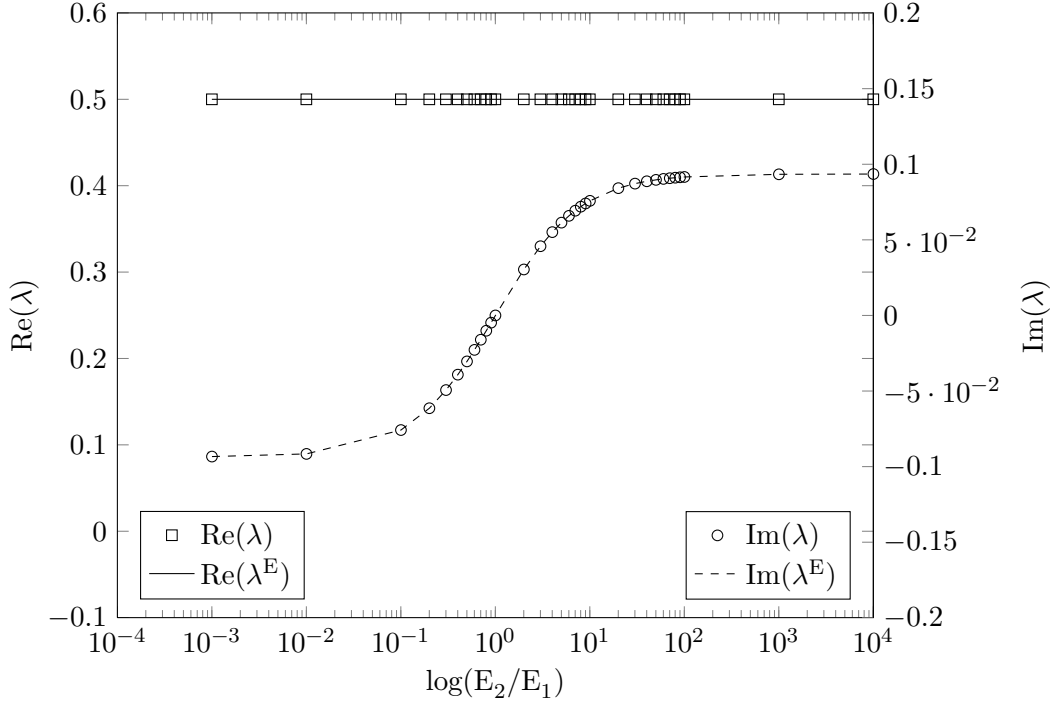


Figure 10: Bimaterial interface crack: order of singularity (λ) as a function of the Young's modulus mismatch.

shape functions of order $p = 9$ are used. All materials are assumed to be homogeneous and isotropic. The computed order of singularity for various combination of material parameters are shown in Figure 13. The results shown in Figure 13 indicate the existence of significant singularities over the full range of E_2/E_1 . The singularities are more severe for higher values of E_2/E_1 than for lower values. Figure 13 also shows the case when the crack is present at the interface of material 3 and material 2. Again, a full range of the order of singularity is shown for various combinations of material parameters. For certain values of E_3/E_2 , multiple real roots are obtained. The present formulation is efficient in capturing the different orders of singularity.

6.2. Crack aligned to the interface

6.2.1. Edge Crack aligned to a bimaterial interface in tension

Consider a bimaterial plate with an edge crack ($a/L = 0.5$) subjected to uniform far field tension ($P = 1$). The geometry, loading and boundary conditions are shown in Figure 14. The material is assumed to be isotropic with Young's modulus $E_1/E_2 = 2$ and Poisson's ratio $\nu_1 = \nu_2 = 0.3$. A state of plane strain is considered in this example. The discontinuities (both the crack and the material interface) are represented independent of the underlying finite element (FE) mesh. From the underlying FE mesh, the scaled boundary region Ω^{sbfem} is identified by

- Selecting the nodes whose nodal support is intersected by the discontinuous surface, viz., crack or the material interface. The nodes whose support are intersected by the material discontinuity are treated within the XFEM framework.
- The elements containing these nodes are then selected. Only the information on the boundary

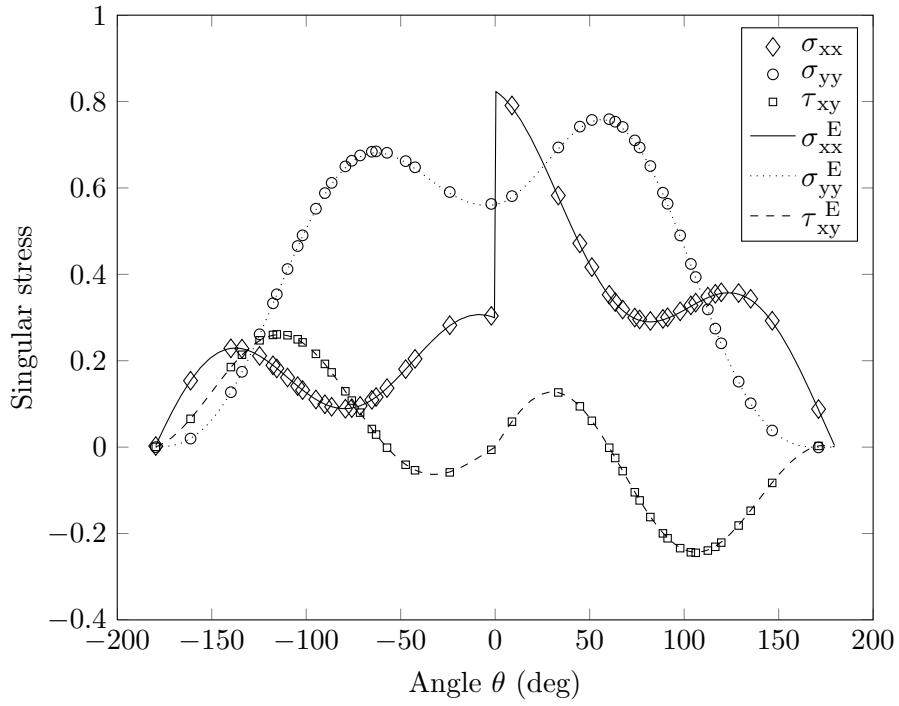


Figure 11: Angular distribution of singular stress ahead of a crack tip for a crack aligned to the bimaterial interface. The ratio of Young's modulus is $E_1/E_2 = 10$. The singular stress fields are obtained for a crack length $a = 0.5$ and $K_I/p\sqrt{\pi a} = 1.123$ and $K_{II}/p\sqrt{\pi a} = -0.123$.

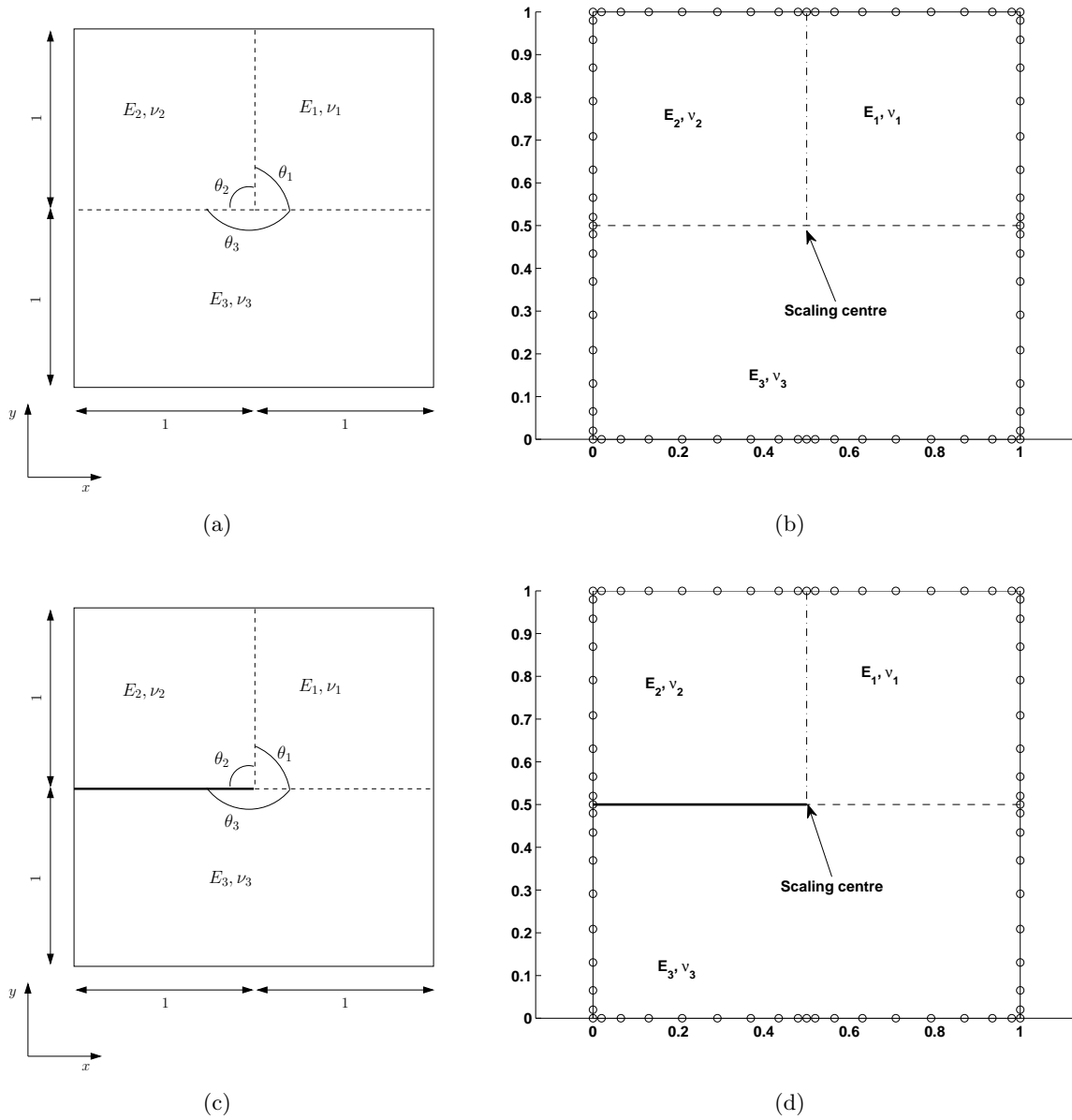
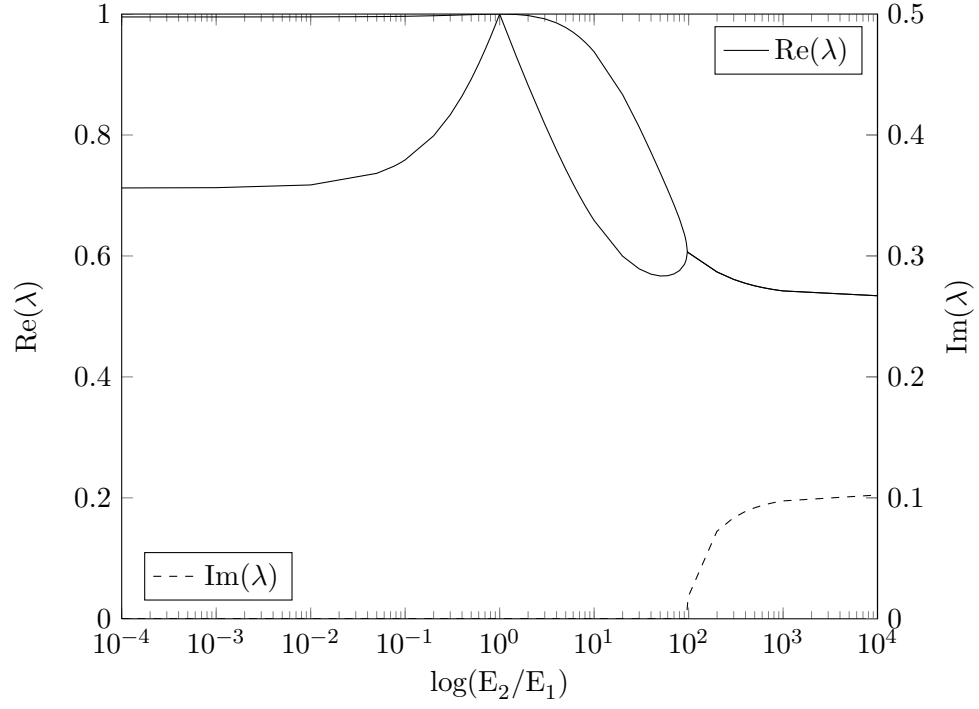
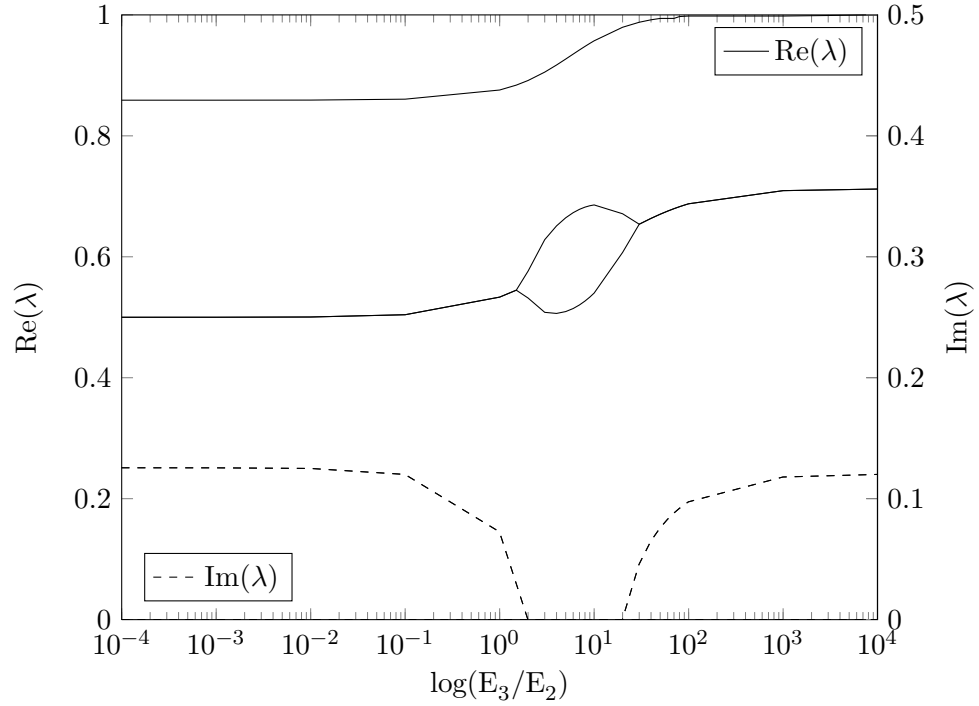


Figure 12: (a-b) a fully bonded triple junction and SBFEM mesh and (c-d) a triple junction with a crack aligned to one of the interfaces.



(a) $E_3/E_1 = 10$, $E_1 = 1$



(b) $E_1/E_2 = 10$, $E_2 = 1$

Figure 13: Order of singularities for a triple junction: (a) a fully bonded junction and (b) a crack along the interface between the material 2 and material 3.

of the domain is retained. The dofs of nodes within the domain are condensed during the solution process.

Within this region, i.e, $\Omega^{\text{sb fem}}$, the scaled boundary formulation is employed to compute the stiffness matrix. Note that no special numerical integration technique is required. The main advantage of this approach is that it does not require a priori knowledge of the asymptotic fields. Figure 15 shows a typical finite element mesh used for this study. The stiffness matrix of the region $A - B - C - D$ is computed by employing the scaled boundary formulation.

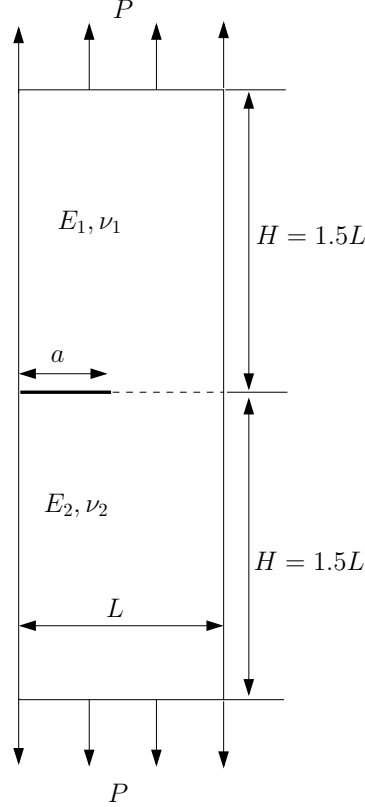
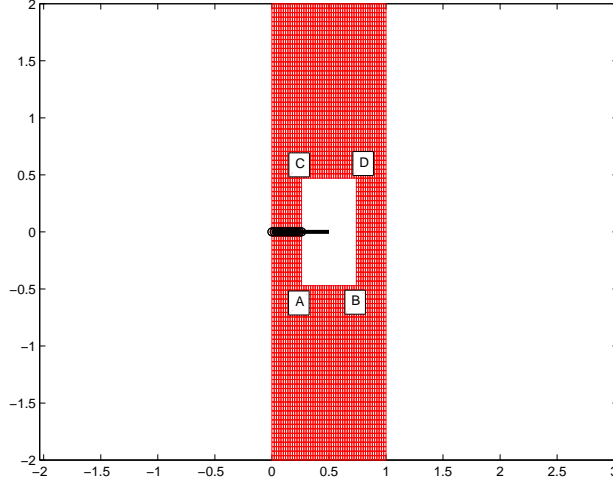
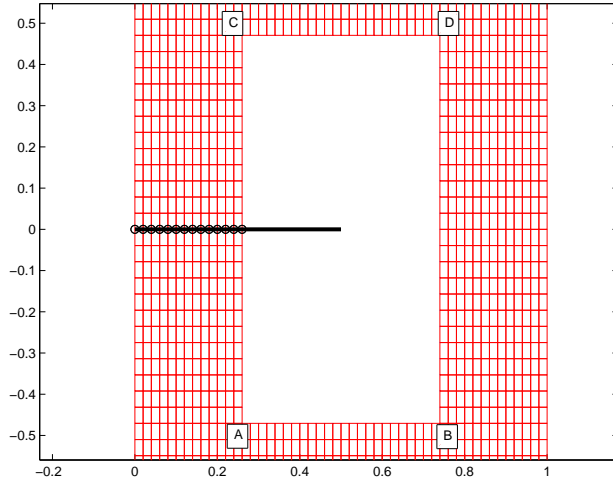


Figure 14: Edge crack aligned to a bimaterial interface in tension: geometry and boundary conditions.

Tables 2 - 3 shows the convergence of the mode I and mode II stress intensity factors with mesh refinement and with number of layers of scaled boundary region in the vicinity of the crack tip. From Table 2 it can be seen that with mesh refinement, the numerical SIF approach a constant value. For this study, 3 layers of elements around the crack tip is replaced with the scaled boundary region. The influence of number of layers on the numerical SIFs is demonstrated in Table 3 for a structured mesh of 51×102 quadrilateral elements. It is noted that with increasing number of layers around the crack tip, the accuracy of the SIFs improve and approach the values reported in the literature based on the boundary element method [57] and the XFEM [41]. It is noted that in [41], first 11 terms of the asymptotic solution were retained. From this study, we can conclude that for a given mesh, 4-5 layers of elements should be replaced with the SBFEM domain for reasonable accuracy. However, for more accurate results, more number of layers can be replaced and represented by the SBFEM.



(a) Discretization for a bimaterial interface crack



(b) Zoomed in view of the region ABCD

Figure 15: A typical discretization for a crack aligned to a bimaterial interface crack. The region ABCD is identified from the FE discretization and then replaced with the SBFEM domain. Note that, the SBFEM domain is constructed from the underlying FE discretization. The dofs of nodes within the SBFEM are suppressed during the solution. In this example, the interface aligns with the element edge. To represent the jump across the crack face, the ‘circled’ nodes are enriched with Heaviside function [40].

Table 2: Edge Crack aligned to a bimaterial interface in tension: Convergence of the mode I and mode II SIFs with mesh refinement. The number of SBFEM layers around the crack tip is 3.

| Number of elements | Number of dofs | Stress Intensity Factors | |
|-----------------------|-------------------|--------------------------|----------|
| | | K_I | K_{II} |
| 11×22 | 459 | 2.7497 | -0.2700 |
| 21×42 | 1769 | 2.7630 | -0.2729 |
| 31×62 | 3879 | 2.7666 | -0.2733 |
| 41×82 | 6789 | 2.7679 | -0.2732 |
| 51×102 | 10499 | 2.7685 | -0.2730 |

Table 3: Edge Crack aligned to a bimaterial interface in tension: Convergence of the mode I and mode II SIFs with number of layers of scaled boundary region in the vicinity of the crack tip. A structured quadrilateral mesh (51×102 elements) was used.

| Number of layers | Stress Intensity Factors | |
|---------------------|--------------------------|----------|
| | K_I | K_{II} |
| 3 | 2.7685 | -0.2730 |
| 4 | 2.8280 | -0.2707 |
| 5 | 2.8219 | -0.2681 |
| 6 | 2.8202 | -0.2674 |
| 7 | 2.8181 | -0.2671 |
| 8 | 2.8170 | -0.2670 |
| Ref. [57] | 2.8190 | -0.2680 |
| Ref. [41] | 2.8440 | -0.2670 |

Crack growth along the interface. In this case, we assume that the crack grows along the interface. Consider a bimaterial plate with an edge crack subjected to uniform tension (see Figure 14). The initial crack length a/L is assumed to be 0.2 and the crack increment at each step is assumed to be 0.2. A structured quadrilateral mesh (51×102) with 5 layers of elements replaced by the SBFEM is used for this study. Like the XFEM, as the crack advances, a new region is identified which is intersected by the discontinuous surface and instead of enriching with additional enrichment functions, the SBFEM is employed to compute the stiffness matrix and for further post-processing of the results. Figure 16 shows the meshes at the initial step and at intermediate steps. The influence of the crack propagation on the numerical stress intensity factors are shown in Figure 17. It is observed that with increasing crack length a/L , the stress intensity factor and the T-stress increases.

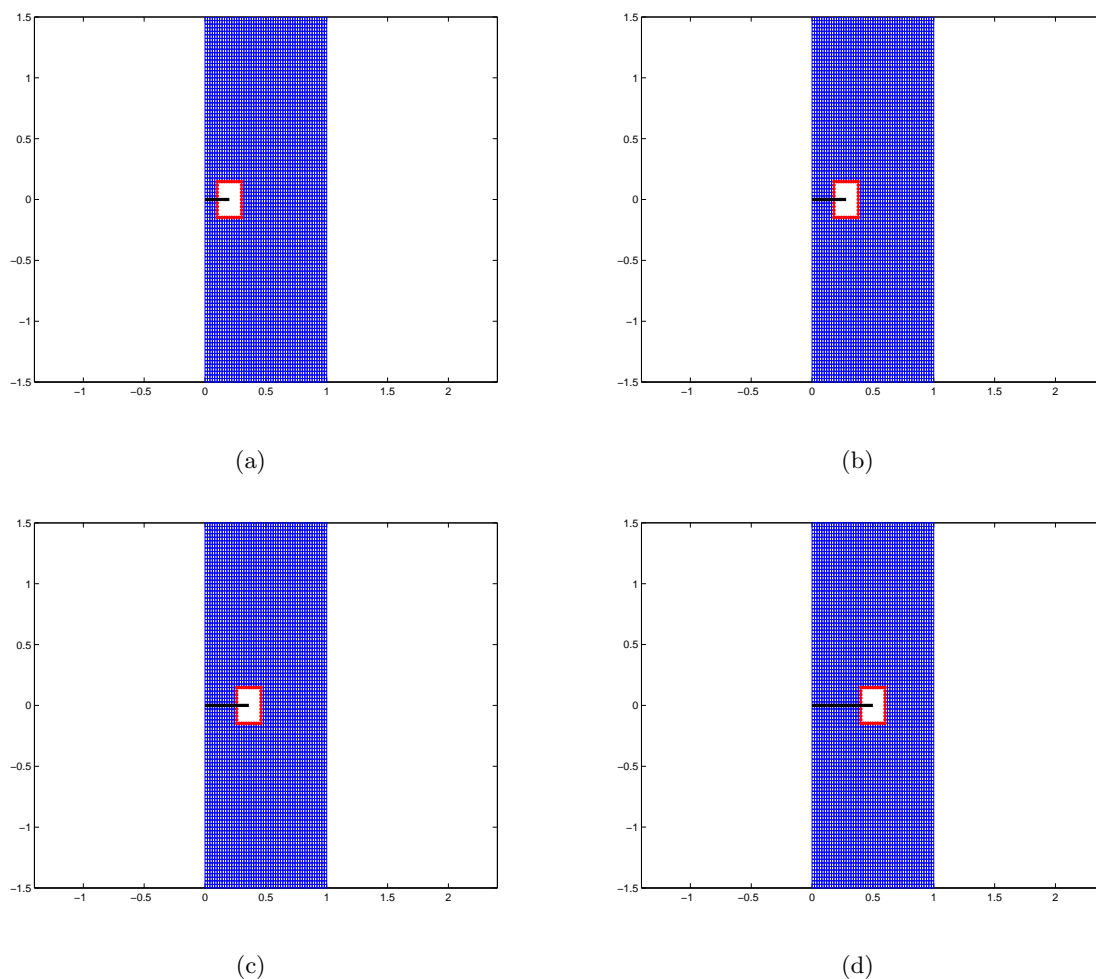
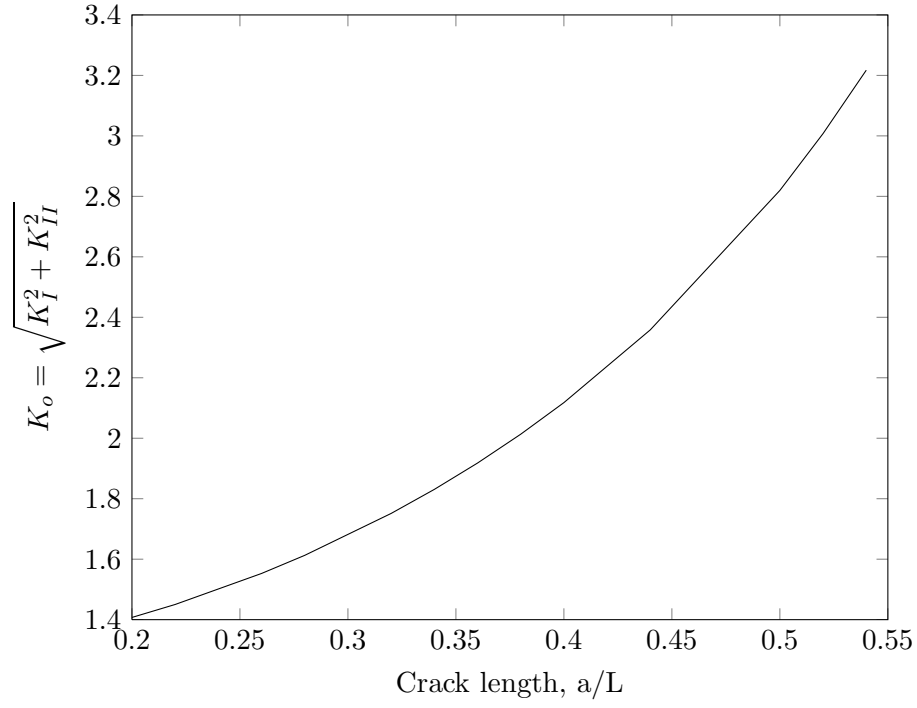
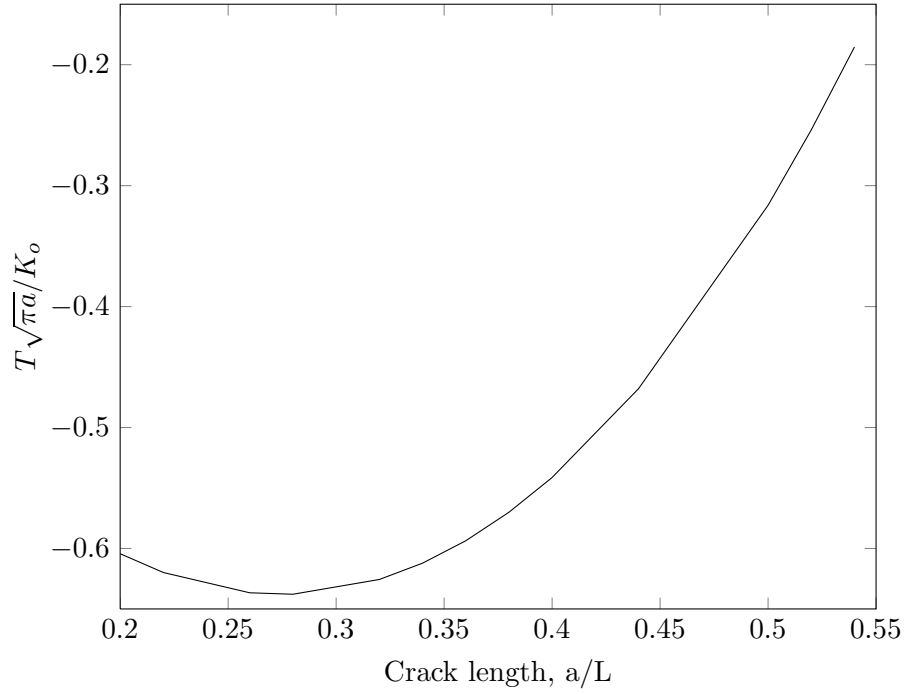


Figure 16: Edge Crack aligned to a bimaterial interface in tension: crack growth along the interface. Meshes at the initial step and at intermediate steps.



(a) Stress intensity factor $K_o = \sqrt{K_I^2 + K_{II}^2}$



(b) T-stress $T\sqrt{\pi a}/K_o$

Figure 17: Crack growth along the interface: the variation of stress intensity factor and T-stress with the increasing crack length, a/L .

6.2.2. Bimaterial plate with a center crack in tension

Consider a bimaterial plate with a center crack subjected to uniform far field tension. The geometry, loading and boundary conditions are shown in Figure 18. The material is assumed to be isotropic with Young's modulus E_1 and E_2 and Poisson's ratio ν_1 and ν_2 . Due to symmetry, only one half of the plate is considered. A state of plane strain is considered in this example. Based on the observation from the previous example, a structured quadrilateral mesh (51×102 elements) with 5 layers of elements were replaced with the SBFEM in the vicinity of the crack tip. The stress intensity factors (K_I, K_{II}) and the T-stress are computed from their definitions (see Section 5).

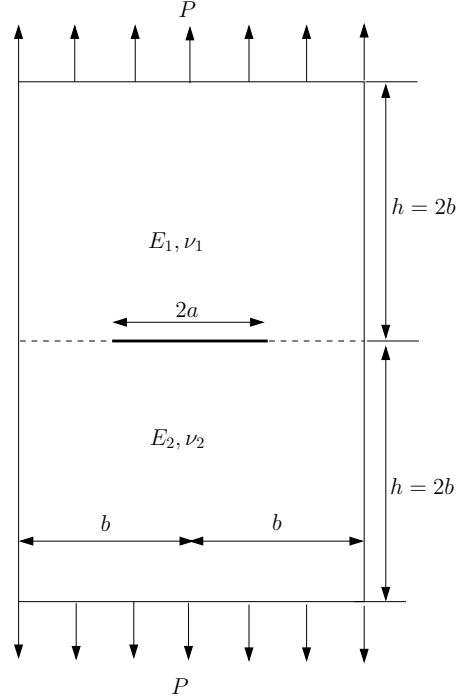


Figure 18: Bi-material plate with a center crack in tension: geometry and boundary conditions.

Table 4: Bimaterial plate with a center crack in tension: Stress intensity factors and the T-stress, where $K_o = \sqrt{K_I^2 + K_{II}^2}$.

| E_1/E_2 | $K_I/\sqrt{\pi a}$ | | $K_{II}/\sqrt{\pi a}$ | | $T\sqrt{\pi a}/K_o$ | | |
|-----------|--------------------|---------|-----------------------|---------|---------------------|-----------|---------|
| | Ref. [53] | Present | Ref. [53] | Present | Ref. [53] | Ref. [55] | Present |
| 1 | 1.189 | 1.1893 | 0.000 | 0.0000 | -1.06 | -1.07 | -1.0552 |
| 2 | 1.179 | 1.1798 | -0.055 | -0.0566 | -0.718 | -0.73 | -0.7144 |
| 5 | 1.148 | 1.1483 | -0.104 | -0.1053 | -0.379 | -0.39 | -0.3770 |
| 10 | 1.123 | 1.1237 | -0.123 | -0.1240 | -0.216 | -0.23 | -0.2147 |

Table 4 presents the stress intensity factors (K_I & K_{II}) and the T-stress for various combinations of material property: $E_1/E_2 = 1, 2, 5$ and 10 for a crack length $a/b = 0.5$. The Poisson's ratio is assumed to be constant with $\nu_1 = \nu_2 = 0.3$. When $E_1/E_2 \neq 1$, the order of the singularity is complex and the stress intensity factors are computed from Equation (41) with the characteristic

length $L = 2a$. The numerically computed stress intensity factors are normalized with $P\sqrt{\pi a}$. The T-stress is evaluated by using Equation (42) to the side of Material 2 (at $\theta = 0^-$) and is normalized with $K_o/\sqrt{\pi a}$. The results from the present formulation are compared with the boundary element technique [55] and with the scaled boundary formulation [53] and a very good agreement is observed. Figure 19 shows the singular stress distribution around the crack tip for Young's modulus ratio $E_1/E_2 = 5$ and the T-stress distribution for various combinations of material property. The singular stresses σ^s and the T-stress are evaluated by using Equation (37) & Equation (42), respectively. It is seen that, as the ratio E_1/E_2 increases, the T-stress increases.

6.2.3. Bimaterial strip with edge loads

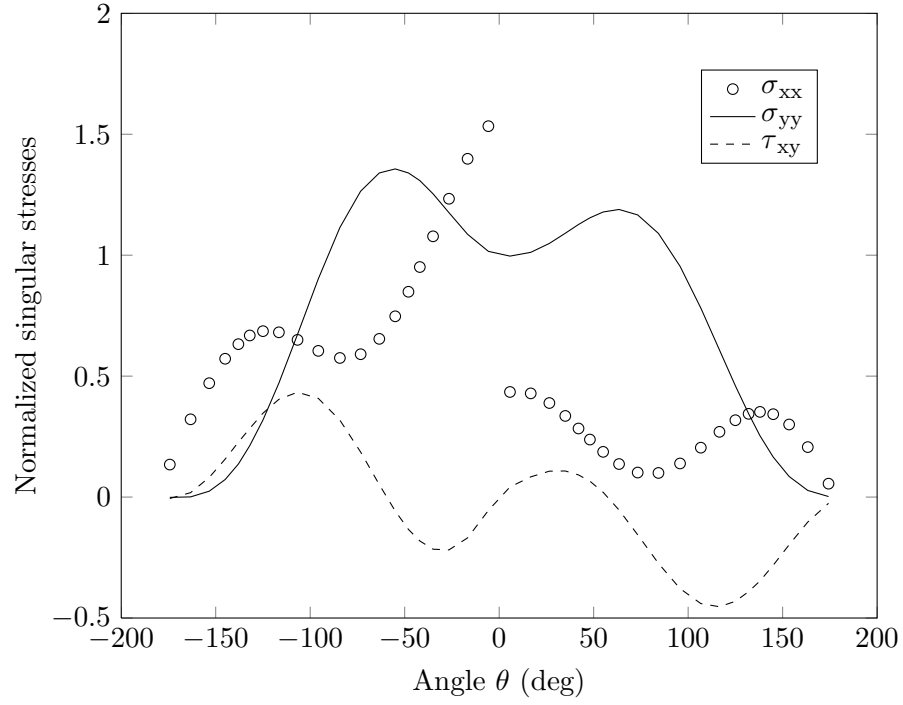
In this example, consider a bimaterial strip constrained at the right end while a concentrated load $P_o = 1$ applied at the left end as shown in Figure 20. The strip contains two layers of thickness h_1 and h_2 and is assumed to be in a state of plane strain condition. The length of the bi-material strip is $L = 10h_2$ and $h_2 = 1$ is considered for this study. A structured mesh of 201×51 quadrilateral elements are considered with 10 layers of elements replaced with the scaled boundary domain. The analytical expression for the T-stress is given in [56]. Table 5 shows the normalized T-stress computed from the current approach for various combinations of material parameters, where T_1 and T_2 are the T-stress evaluated at the side of the material 1 (at $\theta = 0^+$) and the material 2 (at $\theta = 0^-$), respectively. It can be seen that the results from the present formulation are in excellent agreement with the results available in the literature. It is emphasized that the present formulation does not require a priori knowledge of the asymptotic fields.

Table 5: Bimaterial strip with edge loads: material constants and the normalized T-stress. The length of the bimaterial strip, $L = 10h_2$, the crack length $a = L/2$ and concentrated load, $P_o = 1$.

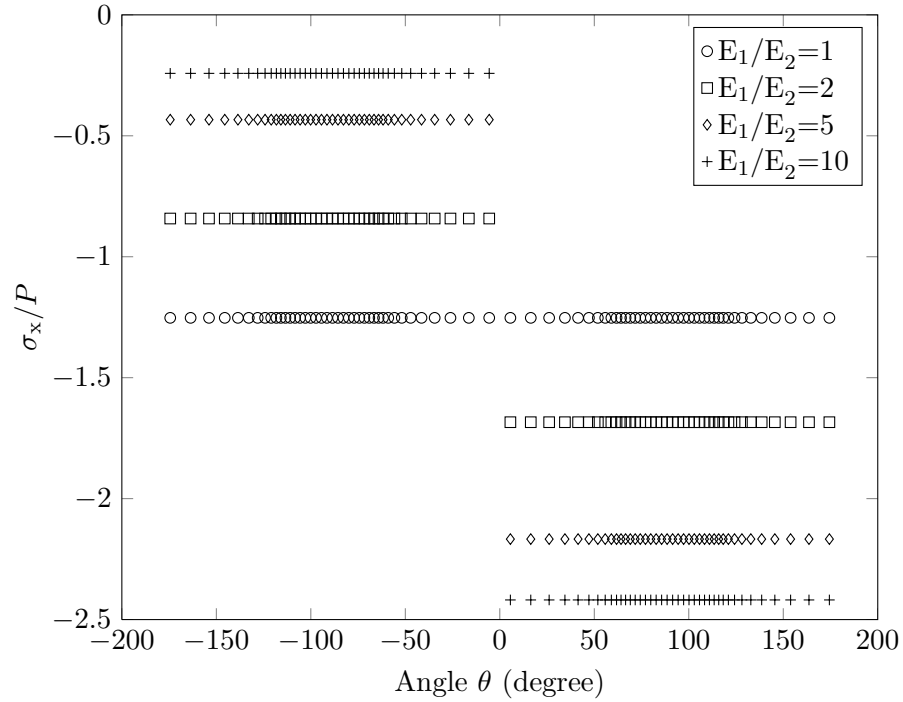
| Case | E_1/E_2 | ν_1 | ν_2 | Ref. [56] | | Ref. [54] | | Present | |
|------|-----------|---------|---------|-----------------------------|-----------------------------|-----------------------------|-----------------------------|-----------------------------|-----------------------------|
| | | | | $T_1^{\text{ref}}/\sigma_o$ | $T_2^{\text{ref}}/\sigma_o$ | $T_1^{\text{ref}}/\sigma_o$ | $T_2^{\text{ref}}/\sigma_o$ | $T_1^{\text{ref}}/\sigma_o$ | $T_2^{\text{ref}}/\sigma_o$ |
| 1 | 7/3 | 1/3 | 1/3 | 0.0709 | 0.0304 | 0.0702 | 0.0301 | 0.07012 | 0.03005 |
| 2 | 20/9 | 1/4 | 1/8 | 0.0784 | 0.0336 | 0.0773 | 0.0331 | 0.07698 | 0.03299 |
| 3 | 4 | 2/5 | 2/5 | 0.1310 | 0.0328 | 0.1317 | 0.0329 | 0.13150 | 0.03288 |
| 4 | 4 | 1/4 | 1/4 | 0.1424 | 0.0356 | 0.1410 | 0.0353 | 0.14081 | 0.03520 |

6.3. Crack terminating at an interface

In this last example, consider a crack terminating at the bimaterial interface. The crack is assumed to be in material 2 and terminating at the interface between the two materials (see Figure 21) and the plate is subjected to a far field tension P . Appropriate Dirichlet boundary conditions are enforced to arrest any rigid body motion. A structured quadrilateral mesh (50×100) with 5 layers of element replaced with the SBFEM is used for this study. Figure 22 shows the stress in the y -direction (σ_{yy} ahead of the crack tip). The results from the present formulation is compared with the stresses computed using a finite element model with a conforming mesh. Figure 23 shows the angular stress distribution ahead of the crack tip for $E_1/E_2 = 100$ and the T-stress distribution for various combination of material properties when the crack is perpendicular to the interface, i.e., $\psi = 0^\circ$. It is seen that, as the ratio E_2/E_1 increases, the T-stress increases. The angular distribution of σ_{yy} for various crack orientation ψ is shown in Figure 24. When the crack is perpendicular to the interface, the stress distribution is symmetric, whilst in any other case it is unsymmetric. It

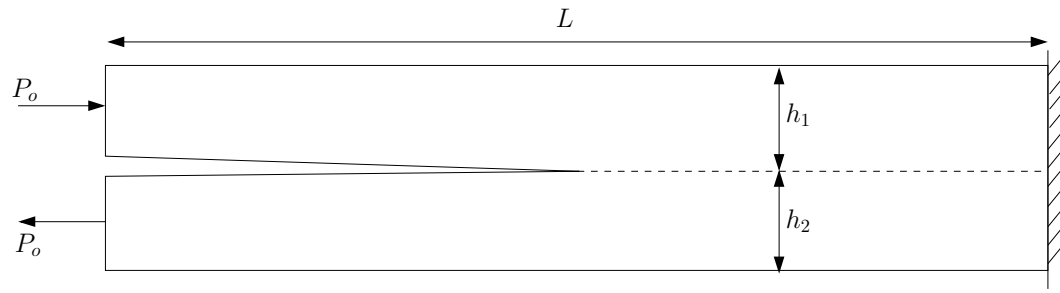


(a)

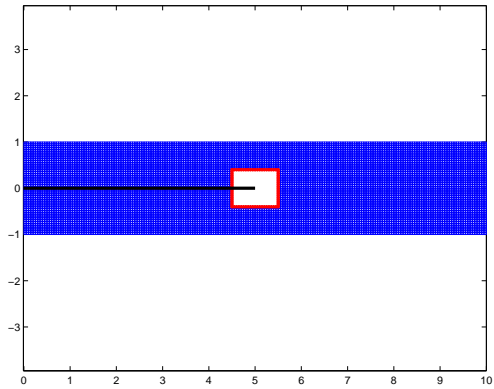


(b)

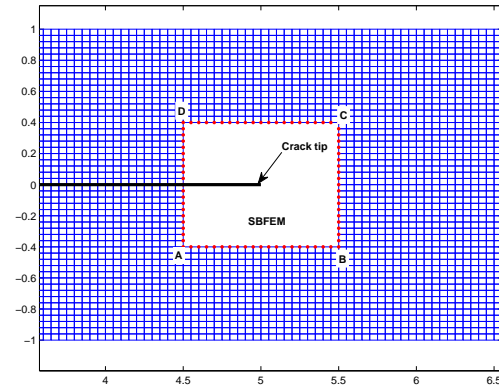
Figure 19: Bimaterial plate with a center crack in tension: (a) Singular stress distribution for $E_1/E_2 = 5$ and (b) the T-stress distribution for various material combinations.



(a)



(b)



(c)

Figure 20: Bi-material strip under edge loads: (a) geometry and boundary conditions; (b) and (c) FE discretization and zoomed in view. The region $A - B - C - D$ is represented by the SBFEM.

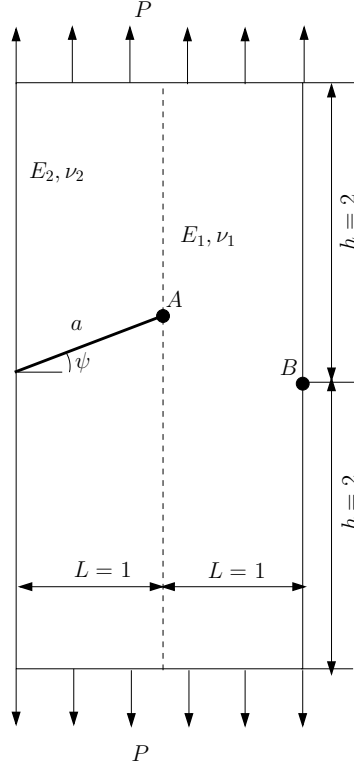


Figure 21: Crack terminating at the material interface: geometry and boundary condition. The crack is assumed to be in material 1 and terminating at the interface between the two materials. ψ is the measured counter clockwise from the positive x axis and determines the inclination of the crack to the interface.

is observed that the crack orientation strongly influences the stress distribution ahead of the crack tip.

Next we consider the case of a crack deflecting into the material. A crack impinging the interface between two dissimilar materials may advance by either propagating along the interface or deflecting into the material. The competition between these two scenarios have been thoroughly dealt in the literature [58, 59, 60, 61]. The material properties are assumed to be $E_2 = 100E_1$. We assume that the initial crack is in material 2 and has deflected into the material 1. In this example, material 1 is homogeneous and isotropic and hence the crack growth is governed by the maximum hoop stress criterion, which states that the crack will propagate from its tip in the direction θ_c where the circumferential stress $\sigma_{\theta\theta}$ is maximum. The critical angle is computed by solving the following equation:

$$K_I \sin \theta_c + K_{II}(3 \cos \theta_c - 1) = 0 \quad (47)$$

Solving Equation (47) gives the crack propagation angle:

$$\theta_c = 2 \arctan \left[\frac{-2 \left(\frac{K_{II}}{K_I} \right)}{1 + \sqrt{1 + 8 \left(\frac{K_{II}}{K_I} \right)^2}} \right] \quad (48)$$

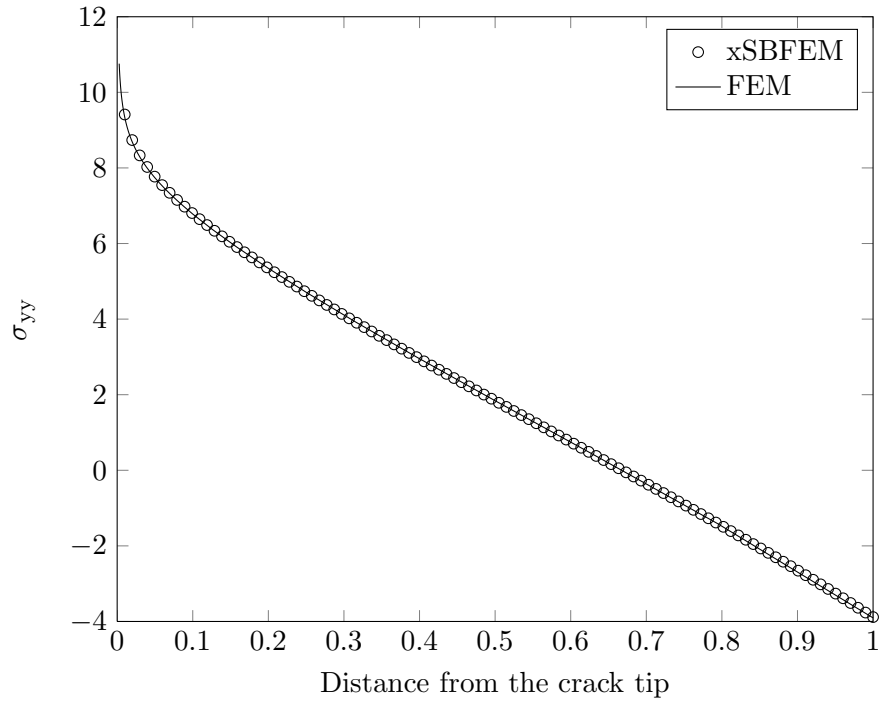
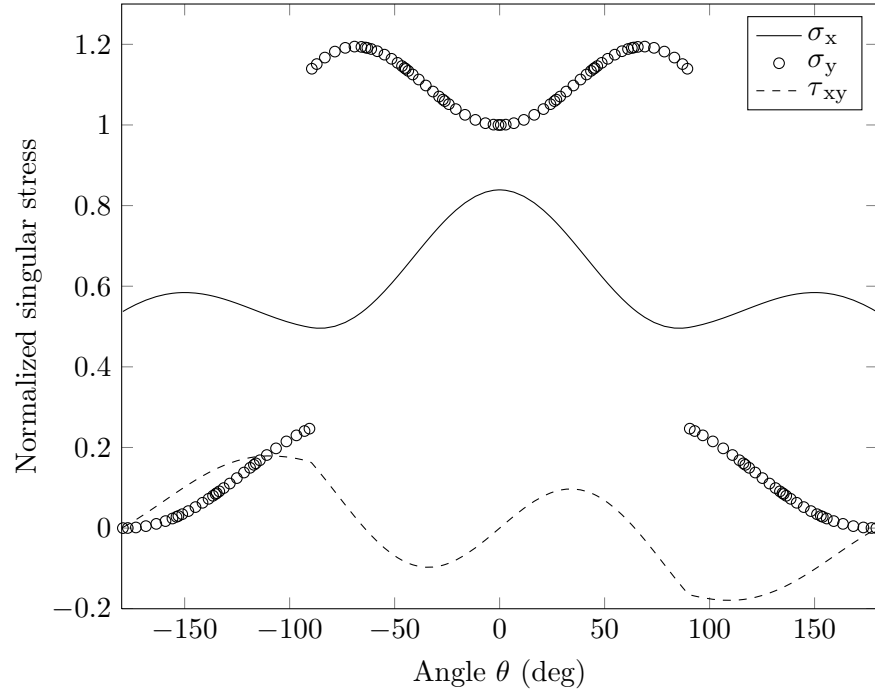
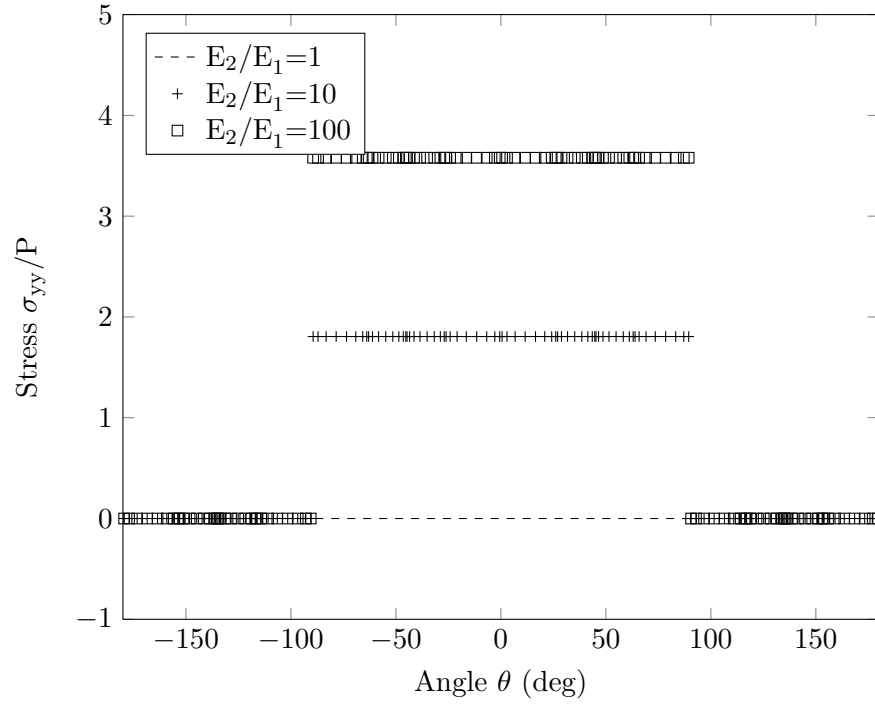


Figure 22: Crack terminating at the material interface: stress σ_{yy} ahead of the crack tip (along the path $A - B$, see Figure 21). The results are compared with the finite element analysis in which a conforming mesh is generated. The ratio of Young's modulus is $E_1/E_2 = 1000$ with $E_2 = 1$.



(a) $E_1/E_2 = 100$



(b)

Figure 23: Angular distribution of singular stresses and T-stress for various combination of material properties for a crack terminating at the material interface.

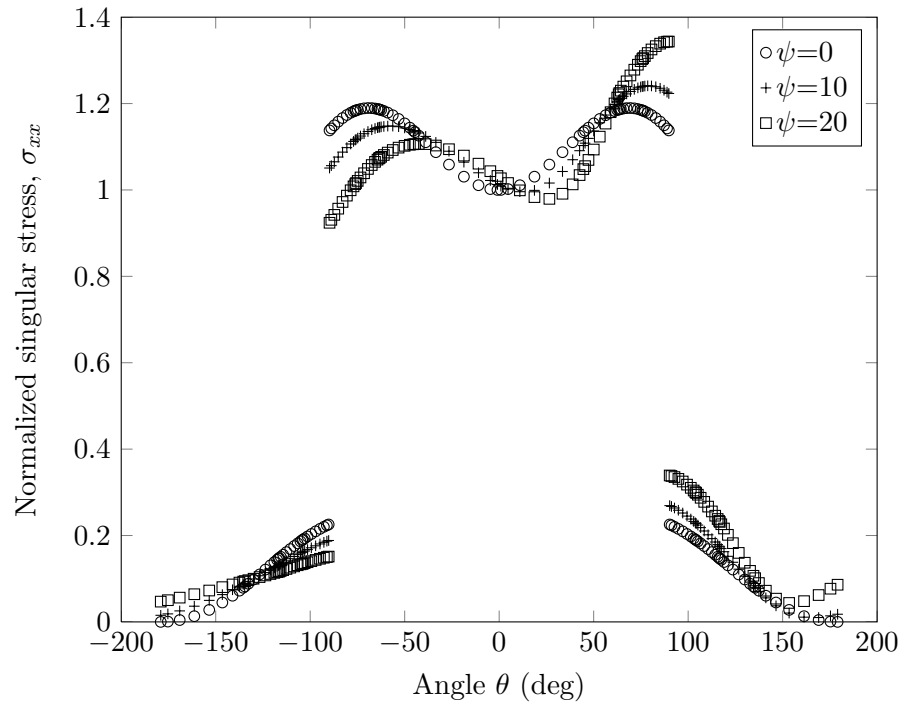


Figure 24: Angular distribution of singular stresses and T-stress for various combination of material properties for a crack terminating at the material interface for various crack orientation. The ratio of Young's modulus is $E_1/E_2 = 100$ with $E_2 = 1$.

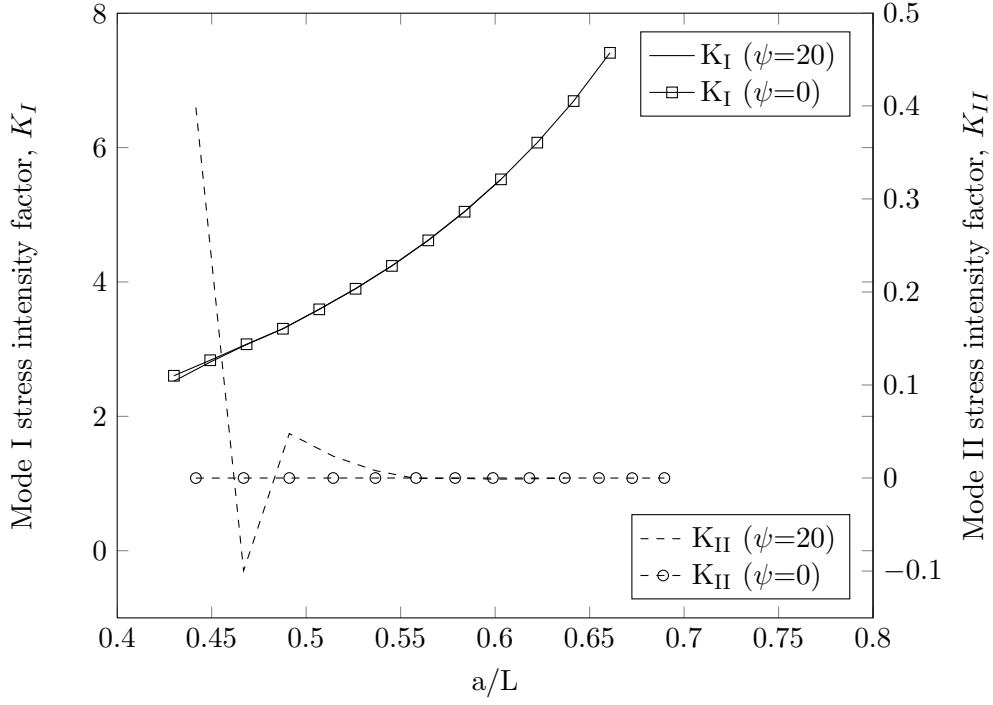


Figure 25: Mode I and II stress intensity factor variation as a function of crack advancement. The crack increment is set in advance and the direction of the crack propagation is computed from Equation (48).

The plate is subjected to a far field tension P (see Figure 21). A structured quadrilateral mesh (51×102) with 5 layers of element replaced with the SBFEM is employed in this example. Figure 25 shows the variation of the stress intensity factors (mode I and mode II) with crack length a/L . The influence of the initial orientation of the crack is also shown. Since the loading is mode I, we expect the crack to grow in a straight line. For a crack impinging at an angle ψ , initially K_{II} is not zero (see Figure 25) and hence the crack advances at an angle that is not equal to zero. However, due to the far field tension, as the crack advances, K_{II} becomes zero and the crack propagates in a straight line. If conventional XFEM was employed, a separate set of enrichment functions should be used when the crack tip lies on the interface and these functions are to be replaced with asymptotic fields for homogeneous material when the crack deflects into the material interface. It is noted that in the extended scaled boundary method, no such modification is necessary and moreover the stress intensity factors and the T-stress can be computed from the definitions.

7. Conclusion

In this paper, we studied the strength of the singularity of cracks aligned to bimaterial interfaces and cracks terminating at the interface by employing a semi-analytical approach. Later, the stress intensity factors and the T-stress was computed by using a combined XFEM and a semi-analytical approach. The salient features of this technique are: (i) no a priori knowledge of the asymptotic fields is required and (ii) the stiffness matrix of the region enriched for a particular crack is obtained directly without a special numerical integration technique. This eliminates the need to compute the enrichment functions as in [26, 28, 29, 31], whilst employing the Heaviside functions allows

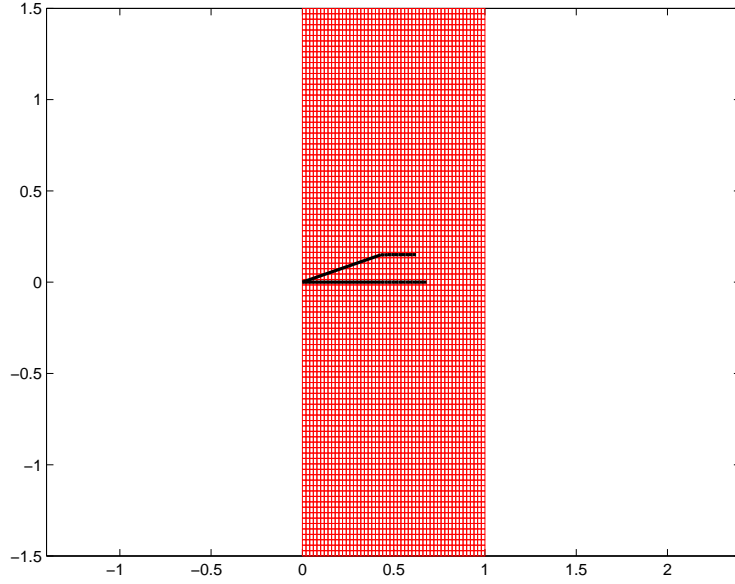


Figure 26: Crack trajectory for a crack impinging at the interface and deflected into material 1. Two cases are considered: (a) a crack perpendicular to the interface and (b) crack oriented at an angle. The solid black line denotes the discontinuous surface.

the discontinuous surfaces to be presented independent of the underlying mesh. The crack growth along the interface and the deflection of the crack into a material is also discussed. The proposed technique can readily be coupled with the existing XFEM/GFEM code and can be applied to study fracture behaviour in heterogeneous materials.

Acknowledgements

S Natarajan would like to acknowledge the financial support of the School of Civil and Environmental Engineering, The University of New South Wales for his research fellowship for the period September 2012 onwards.

References

References

- [1] S. Natarajan, C. Song, Representation of singular fields without asymptotic enrichment in the extended finite element method, *International Journal for Numerical Methods in Engineering* 96 (2013) 813–841.
- [2] R. Barsoum, Triangular quarter-point elements as elastic and perfectly plastic crack tip elements, *International Journal for Numerical Methods in Engineering* 11 (1977) 85–98.
- [3] G. Strang, G. Fix, *An analysis of the finite element method*, Prentice-Hall, 1973.

- [4] D. Tracey, Finite elements for determination of crack-tip elastic stress intensity factors, Tech. Rep. Technical Report AD0732837, Army materials and mechanics research center, Watertown Mass (1971).
- [5] S. Atluri, A. Kobayashi, M. Nakagaki, An assumed displacement hybrid finite element model for linear fracture mechanics, *International Journal of Fracture* 11 (1975) 257–271.
- [6] S. Benzley, Reapplications of singularities with isoparametric finite elements, *International Journal for Numerical Methods in Engineering* 8 (1974) 537–545.
- [7] T. Rabczuk, R. Gracie, J. Song, T. Belytschko, Immersed particle method for fluid-structure interaction, *International Journal for Numerical Methods in Engineering* 81 (2010) 48–71.
- [8] T. Rabczuk, T. Belytschko, Application of particle methods to static fracture of reinforced concrete structures, *International Journal of Fracture* 137 (2006) 19–49.
- [9] T. Rabczuk, G. Zi, S. Bordas, H. Nguyen-Xuan, A geometrically nonlinear three dimensional cohesive crack method for reinforced concrete structures, *Engineering Fracture Mechanics* 75 (2008) 4740–4758.
- [10] G. Zi, T. Rabczuk, W. Wall, Extended meshfree methods without branch enrichment for cohesive cracks, *Computational Mechanics* 40 (2007) 367–382.
- [11] N. V. Bac, H. Nguyen-Xuan, L. Chen, S. Bordas, X. Zhuang, G. Liu, T. Rabczuk, A phantom-node method with edge based strain smoothing for linear elastic fracture mechanics, *Journal of Applied Mathematics*.
- [12] T. Chau-Dinh, G. Zi, P. Lee, J. Song, T. Rabczuk, A phantom-node method for shellmodels with arbitrary cracks, *Computers & Structures* 92–93 (2012) 242–256.
- [13] T. Rabczuk, T. Belytschko, A three-dimensional large deformation meshfree method for arbitrary evolving cracks, *Computer Methods in Applied Mechanics and Engineering* 196 (2007) 2777–2799.
- [14] X. Zhuang, C. Augarde, K. Mathisen, Fracture modeling using meshless methods and level sets in 3D: framework and modeling, *International Journal for Numerical Methods in Engineering* 92 (2012) 969–998.
- [15] T. Rabczuk, G. Zi, S. Bordas, H. Nguyen-Xuan, A simple and robust three dimensional cracking-particle method without enrichment, *Computer Methods in Applied Mechanics and Engineering* 199 (2010) 2437–2455.
- [16] S. Bordas, T. R. and G. Zi, Three-dimensional crack initiation, propagation, branching and junction in nonlinear materials by extrinsic discontinuous enrichment of meshfree methods without asymptotic enrichment, *Engineering Fracture Mechanics* 75 (2008) 943–960.
- [17] T. Rabczuk, S. Bordas, G. Zi, A three-dimensional meshfree method for continuous multiple crack initiation, nucleation and propagation in statics and dynamics, *Computational Mechanics* 40 (2007) 473–495.
- [18] J. Melenk, I. Babuška, The partition of unity finite element method: basic theory and applications, *Computer Methods in Applied Mechanics and Engineering* 39 (1996) 289–314.

- [19] T. Belytschko, T. Black, Elastic crack growth in finite elements with minimal remeshing, *International Journal for Numerical Methods in Engineering* 45 (1999) 601–620.
- [20] O. Garcia, E. Fancello, C. Barcellos, C. Duarte, *hp*-clouds in Mindlin’s thick plate model, *International Journal for Numerical Methods in Engineering* 47 (2000) 1381–1400.
- [21] T. Rabczuk, T. Belytschko, Cracking particles: a simplified meshfree method for arbitrary evolving cracks, *International Journal for Numerical Methods in Engineering* 61 (2004) 2316–2343.
- [22] T. Rabczuk, G. Zi, A. Gerstenberger, W. Wall, A new crack tip element for the phantom-node method with arbitrary cohesive cracks, *International Journal for Numerical Methods in Engineering* 75 (2008) 577–599.
- [23] H. Nguyen-Xuan, G. Liu, S. Bordas, S. Natarajan, T. Rabczuk, An adaptive singular ES-FEM for mechanics problems with singular fields of arbitrary order, *Computer Methods in Applied Mechanics and Engineering* 253 (2013) 252–273.
- [24] T. Belytschko, D. Organ, Y. Krongauz, A coupled finite element - element-free Galerkin method, *Computational Mechanics* 17 (1995) 186–195.
- [25] G. E. Bird, The coupled dual boundary element-scaled boundary finite element method for efficient fracture mechanics, Ph.D. thesis, Durham University (2012).
- [26] C. Duarte, D.-J. Kim, Analysis and applications of a generalized finite element method with global-local enrichment functions, *Computer Methods in Applied Mechanics and Engineering* 197 (2008) 487–504.
- [27] H. Waisman, T. Belytschko, Parametric enrichment adaptivity by the extended finite element method, *International Journal for Numerical Methods in Engineering* 73 (2008) 1671–1692.
- [28] A. Menk, S. Bordas, Numerically determined enrichment functions for the extended finite element method and applications to bi-material anisotropic fracture and polycrystals, *International Journal for Numerical Methods in Engineering* 83 (2010) 805–828.
- [29] S. Mousavi, E. Grinspun, N. Sukumar, Harmonic enrichment functions: A unified treatment of multiple intersecting and branched cracks in the extended finite element method, *International Journal for Numerical Methods in Engineering* 85 (2011) 1306–1322.
- [30] S. Mousavi, E. Grinspun, N. Sukumar, Higher-order extended finite elements with harmonic enrichment functions for complex crack problems, *International Journal for Numerical Methods in Engineering* 86 (2011) 560–574.
- [31] Q.-Z. Zhu, On enrichment functions in the extended finite element method, *International Journal for Numerical Methods in Engineering* 91 (2012) 186–217.
- [32] Q. Xiao, B. Karihaloo, Implementation of hybrid crack element on a general finite element mesh and in combination with XFEM, *Computer Methods in Applied Mechanics and Engineering* 196 (2007) 1864–1873.

- [33] E. Chahine, P. Laborde, Y. Renard, Spider XFEM, an extended finite element variant for partially unknown crack-tip displacement, *European Journal of Computational Mechanics* 17 (2008) 625–636.
- [34] J. Réthore, S. Roux, F. Hild, Hybrid analytical and extended finite element method (HAX-FEM): A new enrichment procedure for cracked solids, *International Journal for Numerical Methods in Engineering* 81 (2010) 269–285.
- [35] I. Babuška, U. Banerjee, Stable generalized finite element method (SSGFEM), *Computer Methods in Applied Mechanics and Engineering* 201–204 (2012) 91–11.
- [36] A. Asadpoure, S. Mohammadi, A new approach to simulate the crack with the extended finite element method in orthotropic media, *International Journal for Numerical Methods in Engineering* 69 (2007) 2150–2172.
- [37] S. E. Ashari, S. Mohammadi, Delamination analysis of composites by new orthotropic bi-material extended finite element method, *International Journal for Numerical Methods in Engineering* 86 (2011) 1507–1543.
- [38] G. Hattori, R. Rojas-Díaz, A. Sáez, N. Sukumar, F. Garcia-Sánchez, New anisotropic crack-tip enrichment functions for the extended finite element method, *Computational Mechanics* 50 (2012) 591–601.
- [39] J. Dolbow, M. Gosz, On the computation of mixed-mode stress intensity factors in functionally graded materials, *International Journal of Solids and Structures* 39 (2002) 2557–2574.
- [40] N. Sukumar, Z. Huang, J.-H. Prévost, Z. Suo, Partition of unity enrichment for bimaterial interface cracks, *International Journal for Numerical Methods in Engineering* 59 (2004) 1075–1102.
- [41] X. Liu, Q. Xiao, B. Karihaloo, XFEM for direct evaluation of mixed mode SIFs in homogeneous and bi-material, *International Journal for Numerical Methods in Engineering* 59 (2004) 1103–1118.
- [42] L. Bouhala, Q. Shao, Y. Koutsawa, A. Younes, P. N. nez, A. Makradi, S. Belouettar, An XFEM crack-tip enrichment for a crack terminating at a bi-material interface, *Engineering Fracture Mechanics* 102 (2013) 51–64.
- [43] J. Kim, G. Paulino, The interaction integral for fracture of orthotropic functionally graded materials: evaluation of stress intensity factors, *International Journal of Solids and Structures* 40 (2003) 3967–4001.
- [44] S. Courtin, C. Gardin, C. Bézine, H. Hamouda, Advantages of the J-integral approach for calculating stress intensity factors when using the commercial finite element software ABAQUS, *Engineering Fracture Mechanics* 72 (2005) 2174–2185.
- [45] J. Berger, A. Karageorghis, P. Martin, Stress intensity factor computation using the method of fundamental solutions: Mixed-mode problems, *International Journal for Numerical Methods in Engineering* 69 (2007) 469–483.
- [46] A. de Morais, Calproblems of stress intensity factors by the force method, *Engineering Fracture Mechanics* 74 (2007) 739–750.

- [47] J. Passieux, A. Gravouil, J. Réthoré, Direct estimation of generalized stress intensity factors using a three-scale concurrent multigrid X-FEM, *International Journal for Numerical Methods in Engineering* 85 (2011) 1648–1666.
- [48] J. Wolf, C. Song, The scaled boundary finite-element method - a fundamental solution-less boundary element method, *Computer Methods in Applied Mechanics and Engineering* 190 (2001) 5551–5568.
- [49] A. Deeks, J. Wolf, A virtual work derivation of the scaled boundary finite element method for elastostatics, *Computational Mechanics* 28 (2002) 489–594.
- [50] E. T. Ooi, C. Song, F. Tin-Loi, Z. Yang, Polygon scaled boundary finite elements for crack propagation modeling, *International Journal for Numerical Methods in Engineering* 91 (2012) 319–342.
- [51] S. Natarajan, E. T. Ooi, I. Chiong, C. Song, Convergence and accuracy of displacement based finite element formulations over arbitrary polygons: Laplace interpolants, strain smoothing and scaled boundary polygon formulation, *Finite Elements in Analysis and Design* Accepted in press.
- [52] M. Williams, On the stress distribution at the base of a stationary crack, *Journal of Applied Mechanics*, ASME 24 (1957) 109–114.
- [53] C. Song, Evaluation of power-logarithmic singularities, T-stress and higher order terms of in-plane singular stress field at cracks and multi-material corners, *Engineering Fracture Mechanics* 72 (2005) 1498–1530.
- [54] H. Yu, L. Wu, H. Li, T-stress evaluation of an interface crack in the materials with complex interfaces, *International Journal of Fracture* 177 (2012) 25–37.
- [55] J. Sladek, V. Sladek, Evaluations of the T-stress for interface cracks by the boundary element method, *Engineering Fracture Mechanics* 56 (1997) 813–825.
- [56] J. Kim, J. Vlassak, T-stress of a bi-material strip under generalized edge loads, *International Journal of Fracture* 142 (2006) 315–322.
- [57] T. Matsumoto, M. Tanaka, R. Obara, Computation of stress intensity factors of interface cracks based on interaction energy release rates and BEM sensitivity analysis, *Engineering Fracture Mechanics* 65 (2000) 683–702.
- [58] M.-Y. He, J. W. Hutchinson, Crack deflection at an interface between dissimilar elastic materials, *International Journal of Solids and Structures* 25 (1989) 1053–1067.
- [59] M.-Y. He, J. W. Hutchinson, materials a crack out of an interface, *Journal of Applied Mechanics* 56 (1989) 270–278.
- [60] J. W. Hutchinson, Z. Suo, Mixed mode cracking in layered materials, *Adv. Appl. Mech.* 29 (1992) 63–191.
- [61] Z. Zhang, Z. Suo, Split singularities and the competition between crack penetration and debond at a bimaterial interface, *International Journal of Solids and Structures* 44 (2007) 4559–4573.